Four-Hole-Line Diagrams in Nuclear Matter*

B. D. DAY

Argonne National Laboratory, Argonne, Illinois 60439

(Received 30 June 1969)

The Brueckner-Goldstone diagrams with four independent hole lines, which give the third term in the expansion for the ground-state energy of infinite nuclear matter, are enumerated. These diagrams are grouped in a natural way into 16 distinct classes. Only one of these classes (the four-body clusters) involves the solution of a four-body equation. Six classes require the solution of the three-body Bethe-Faddeev equations, and nine classes can be evaluated in terms of two-body matrix elements alone. Exact formal expressions are given for the contribution to the energy from each class of diagrams. In these expressions, all exchange diagrams are included, and all energy denominators are clearly defined. Numerical estimates are made for each class of diagrams, assuming the two-body interaction to be the Reid soft-core potential. The sum of all contributions is attractive and is about 0.6–1.6 MeV. Most of the uncertainty in this result is caused by omission of the tensor force in certain diagrams. The implications of these results for the convergence of the energy expansion are discussed.

I. INTRODUCTION

A WIDELY accepted method of calculating the ground-state energy of infinite nuclear matter is to group the diagrams in the Brueckner–Goldstone[1] expansion according to the number of independent hole lines.[2–5] Diagrams with two independent hole lines (these are just the first-order diagrams) give the first term in the expansion, three-hole-line diagrams give the second term, etc. The convergence of this expansion is roughly governed[4,5] by a parameter κ that is equal to the particle density times the wound integral of the two-body wave function. The magnitude of κ is one-fifth to one-seventh for currently fashionable nucleon-nucleon potentials at normal density.[6] The evaluation of the first-order diagrams requires the calculation of the reaction matrix (G matrix). This has been studied by many authors (see, for example, Refs. 6–10) and no longer presents any serious difficulty. A certain amount of work has also been done on the three-hole-line terms.[3,11–16] Certain four-hole-line diagrams have been investigated, but no systematic study has previously been made of these diagrams. In this paper the results of such a study are given. The four-hole-line diagrams are enumerated, and quantitative estimates are made of their contributions to the binding energy.

The purpose of studying the four-hole-line diagrams is to find out how well the hole-line expansion converges. The two-hole-line diagrams contribute about -33 MeV per particle,[6] and the three-body cluster terms give about -1 MeV.[14] The latter figure is surprisingly small. One would have expected to obtain roughly κ times the two-hole-line contribution, i.e., about 5 MeV. Similarly, one might expect the contribution of a typical four-hole-line diagram to be κ^2 times the two-hole-line term, i.e., about 0.7 MeV. Since there are a great many different classes of four-hole-line diagrams, their sum could easily amount to several MeV. Clearly the four-hole-line diagrams must be carefully investigated before the results of the theory can be trusted to better than 3 or 4 MeV per particle.

Baker and his co-workers[17] have proposed and developed a procedure for summing the perturbation series that differs from the hole-line expansion. Nothing is said here about the relative merits of these two methods. We simply assume the hole-line expansion to be correct and study the four-hole-line diagrams.

The present work is applicable only to two-body potentials that contain a very strong short-range repulsion, e.g., the potentials of Reid[18] and of Hamada and Johnston.[19] For relatively smooth and weak potentials, ordinary perturbation theory in powers of the potential can be used, and the hole-line expansion is not needed. Examples of such potentials are the Tabakin

* Work performed under the auspices of the U.S. Atomic Energy Commission.

[1] J. Goldstone, Proc. Roy. Soc. (London) **A239**, 267 (1957).
[2] R. Rajaraman, Phys. Rev. **131**, 1244 (1963).
[3] H. A. Bethe, Phys. Rev. **138**, B804 (1965).
[4] B. D. Day, Rev. Mod. Phys. **39**, 719 (1967).
[5] B. H. Brandow, Phys. Rev. **152**, 863 (1966).
[6] A. Kallio and B. D. Day, Nucl. Phys. **A124**, 77 (1969).
[7] G. Dahll, E. Ostgaard, and B. Brandow, Nucl. Phys. **A124**, 481 (1969).
[8] H. A. Bethe, B. H. Brandow, and A. G. Petschek, Phys. Rev. **129**, 225 (1963).
[9] S. A. Moszkowski and B. L. Scott, Ann. Phys. (N. Y.) **11**, 65 (1960).
[10] K. A. Brueckner and J. L. Gammel, Phys. Rev. **109**, 1023 (1958). BGT stands for Brueckner-Gammel-Thaler.
[11] H. A. Bethe, Phys. Rev. **158**, 941 (1967).
[12] B. Day, Phys. Rev. **151**, 826 (1966).
[13] M. W. Kirson, Nucl. Phys. **A99**, 353 (1967).
[14] R. Rajaraman and H. A. Bethe, Rev. Mod. Phys. **39**, 745 (1967).
[15] B. S. Bhakar and R. J. McCarthy, Phys. Rev. **164**, 1343 (1967).
[16] Y. Akaishi, H. Bando, A. Kuriyama, and S. Nagata, Progr. Theoret. Phys. (Kyoto) **40**, 288 (1968).
[17] G. A. Baker, Jr., Phys. Rev. **131**, 1869 (1963); G. A. Baker, Jr., J. L. Gammel, and B. J. Hill, *ibid.* **132**, 1373 (1963); G. A. Baker, Jr., *ibid.* **140**, B9 (1965); G. A. Baker, Jr., and J. Kahane, J. Math. Phys. **10**, 1647 (1969).
[18] R. V. Reid, Ann. Phys. (N. Y.) **50**, 411 (1968).
[19] T. Hamada and I. D. Johnston, Nucl. Phys. **34**, 382 (1962).

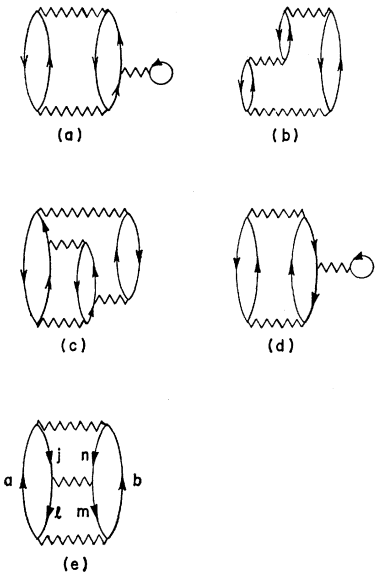

FIG. 1. Diagrams with three independent hole lines.

potential[20,21] and the potential developed by Nestor, Davies, Krieger, and Baranger[22] for use in Hartree-Fock calculations.

A brief examination of the familiar three-hole-line diagrams will show us what types of four-hole-line diagrams can be expected to arise. The three distinct classes of three-hole-line diagrams are shown in Fig. 1. Figures 1(a)–1(c) are three members of the class of (infinitely many) three-body cluster diagrams. In a typical three-body cluster diagram, three particles scatter out of the Fermi sea, interact among themselves any number of times, and then fall back into the sea. Calculating the sum of this class of diagrams therefore requires the solution of a three-body equation.[3]

The other two classes of three-hole-line diagrams are of a completely different type. One of these classes consists of the hole-bubble diagram [Fig. 1(d)], and the other consists of the hole-hole diagram [Fig. 1(e)]. The hole-hole diagram has four hole lines, but momentum conservation in the middle G matrix reduces the number of *independent* hole lines to three. Since the hole-hole class contains only a single diagram, its contribution can be calculated in terms of a small number of *two-body* matrix elements. This is in contrast to the three-body clusters, where summing the series introduces a *three-body* wave function. Whenever three particles are excited above the sea, they must be allowed to interact any number of times, and a three-body wave function will inevitably appear. But in the hole-hole diagram, the particles interact two at a time, and at no point are three particles simultaneously excited above the sea. So we call the hole-hole diagram a two-body combination diagram. The hole-bubble diagram is also a two-body combination diagram. In practice, the hole-bubble diagram is canceled by the self-consistent single-particle potential, and the hole-hole diagram contributes less than 1 MeV per particle.

In a similar way, each class of four-hole-line diagrams will be classified as a two-body combination class, a three-body combination class, or a four-body cluster class. Two-body combination diagrams involve only two-body matrix elements. Three-body combination diagrams involve three-body matrix elements (obtained by solving a three-body equation). The four-body cluster diagrams require the solution of a four-body equation. In the language of Brandow,[5] the two-body and three-body combination diagrams have more than one "irreducible compact part," and the sum of all four-body cluster diagrams consists of a single irreducible compact part with four external lines.

In Sec. II the four-hole-line diagrams are enumerated, and formal expressions are given for their contributions to the binding energy. In Sec. III, we make numerical estimates of these contributions. The results of the calculations are discussed in Sec. IV.

II. ENUMERATION OF DIAGRAMS

A. Two-Body Combination Diagrams

Before setting down the two-body combination diagrams, we describe our notation and make some preliminary remarks. The G matrix is a two-body operator defined by

$$G=v-v(Q/e)G, \tag{2.1}$$

where the projection operator Q requires both particles to be above the Fermi sea, and e is defined by

$$e\mid pq\rangle=(E_p+E_q-W)\mid pq\rangle. \tag{2.2}$$

Here, E_p and E_q are the single-particle energies of the plane-wave states p and q, respectively. (Unless otherwise indicated, we use $a, b, c, \ldots, h$ to label states above the sea, $i, j, \ldots, n$ for states in the sea, and $p, q, r, \ldots$, for states that could be either in the sea or above it.)

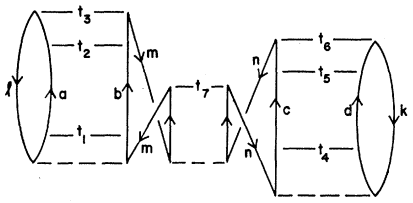

FIG. 2. Goldstone diagram to which GTO can be applied. Diagrams of this type are summed by means of GTO into the diagram of class A1.

[20] F. Tabakin, Ann. Phys. (N. Y.) **30**, 51 (1964).
[21] J. J. MacKenzie, Phys. Rev. **179**, 1002 (1969).
[22] C. W. Nestor, K. T. R. Davies, S. J. Krieger, and M. Baranger, Nucl. Phys. **A113**, 14 (1968).

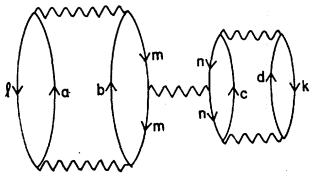

FIG. 3. Four-hole-line diagram of class A1.

We see that G and e both depend on the starting energy W. We use $G(lm)$, $e(lm)$ to represent these quantities calculated with starting energy E_l+E_m. Also, $G(lmn;\ a)$ corresponds to $W=E_l+E_m+E_n-E_a$, and similarly for $e(lmn;\ a)$.

The symbol $\sum$ with no indices underneath implies the summation over all indices of the expression following the $\sum$. For example, $\sum F(a,\ l,\ p)$ means the sum of $F(a,\ l,\ p)$ over states a above the Fermi sea, states l in the Fermi sea, and all states p. But the notation $\sum_{ap} F(a,\ l,\ p)$ implies summation over a and p with l remaining fixed.

Exchange diagrams will be treated by means of the following useful method of Brandow[23] and Hugenholtz.[24] Only one Goldstone diagram will be shown from each group of diagrams that are obtained one from another by successively exchanging the incoming (or outgoing) lines in two-body interactions. But in writing the contribution from this diagram each direct matrix element is replaced by the corresponding direct-minus-exchange matrix element. Then a factor $\frac{1}{2}$ is inserted for each pair of equivalent lines. Two lines are equivalent if they both start at the same interaction, both end at the same interaction, and both run in the same direction. For example, in Fig. 1(e) there are three pairs of equivalent lines—(lm), (jn), and (ab).

Another useful rule is the following: One Goldstone diagram can be obtained from another by exchange if, and only if, the two diagrams are identical in the Hugenholtz[24] representation.

This method of including exchange is well suited only for two-body-combination diagrams. Another method will be used for classes of diagrams involving three-body and four-body matrix elements.

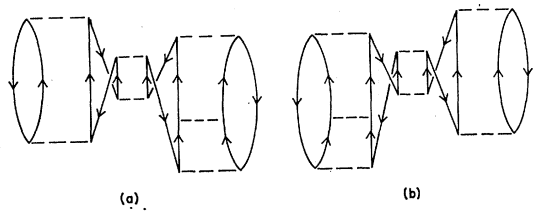

FIG. 4. Diagrams illustrating that double counting occurs when GTO is applied to Fig. 2.

[23] B. H. Brandow, Rev. Mod. Phys. **39**, 771 (1967).
[24] N. M. Hugenholtz, Physica **23**, 481 (1957).

In the two-body combination diagrams, we will often replace a direct-minus-exchange matrix element of G by twice the direct matrix element. For example, expression (2.4) contains two direct matrix elements. But if each is replaced by one-half of the direct-minus-exchange matrix element, the value of (2.4) is unchanged, and the result is in accord with Brandow's rule. When all exchange terms are included, the contribution from any diagram, regardless of whether or not it is a two-body combination diagram, must remain unchanged when a direct matrix element of G is replaced by one-half the direct-minus-exchange matrix element.

The over-all sign of the contribution of any diagram is[1,4] $(-1)^{h+l+e}$, where h is the number of hole lines, l is the number of closed loops, and e is the number of (positive definite) energy denominators.

Many four-hole-line diagrams have more than four hole lines. But after momentum conservation has been taken into account, the number of *independent* hole lines is, by definition, equal to four. We will make extensive use of the preceding ideas from now on.

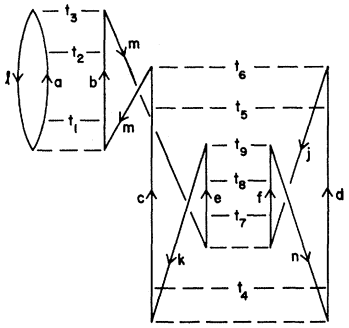

FIG. 5. Goldstone diagram to which GTO can be applied. Diagrams of this type are summed by means of GTO into the diagrams of class A2.

The idea of generalized time ordering (GTO) is used extensively in our discussion of two-body combination diagrams. The GTO procedure collapses large classes of diagrams with conventional Brueckner-Goldstone energy denominators into single diagrams with simpler energy denominators. A well-known example[4,8] is the hole-bubble diagram of Fig. 1(d), in which the GTO procedure puts the middle G matrix on the energy shell. Discussions of GTO can be found in Appendix B of Ref. 8, and on pages 777–778 of Ref. 23.

We must apply GTO to structures such as the one in Fig. 2, in which the dashed lines represent the two-body potential v. Note that GTO is applied *before* ladders of v interactions are summed into G matrices (represented by wavy lines, as in Fig. 1). Each interaction is labeled by a time t_i. We think of time increasing in the upward direction so that $t_i>t_j$ simply means that

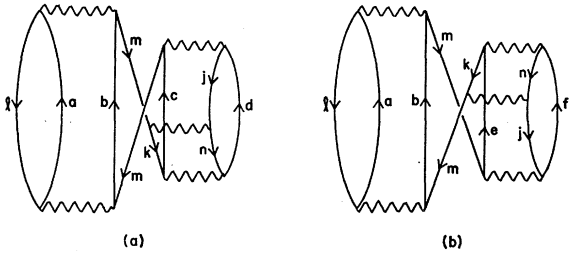

FIG. 6. Four-hole-line diagrams of class A2.

the interaction labeled t_i occurs above the interaction labeled t_j.

The topology of Fig. 2 implies that within any one of the three ladders the time order is fixed, e.g., we must have $t_1<t_2<t_3$. But there is a lot of freedom for the relative time orders of interactions in different ladders. For example, we can equally well have $t_2<t_6$ or $t_2>t_6$, and each possiblity corresponds to a distinct Goldstone diagram. On the other hand, the interaction just below t_1 *must* occur below t_7. This is necessary in order that the line m connecting this interaction to t_7 remain a hole line and not become an upgoing (particle) line. Our task is to use GTO to include each Goldstone diagram contained in Fig. 2 (and in other structures) exactly once.

Class A1. All diagrams that can be obtained from Fig. 2, subject to the time restrictions

$$t_1<t_7<t_2, \qquad t_4<t_7<t_5, \tag{2.3}$$

are assigned to class A1. The GTO treatment reduces the entire class to the single diagram shown in Fig. 3. Its contribution to the energy is

$$\begin{aligned} W(\mathrm{A1}) = A^{-1}\tfrac{1}{2}\sum & \langle lm \mid G(lm)[Q/e(lm)] \mid ab\rangle \\ & \times\langle ab \mid [Q/e(lm)]G(lm) \mid lm-ml\rangle \\ & \times\langle nk \mid G(nk)[Q/e(nk)] \mid cd\rangle\langle cd \mid [Q/e(nk)] \\ & \times G(nk) \mid nk-kn\rangle\langle mn \mid G(mn) \mid mn-nm\rangle. \end{aligned} \tag{2.4}$$

Here, A is the total number of particles, and $W(\mathrm{A1})$ is the energy per particle from class A1. This notation will be used from now on. Note that the GTO has put all the G matrices on the energy shell.

The factor $\frac{1}{2}$ in (2.4) is necessary because the time restrictions (2.3) count each distinct Goldstone diagram twice. For example, the two diagrams shown in Fig. 4 are *not* distinct, but each is counted separately in the GTO treatment.

Brandow[5] has emphasized that class A1 can be considered to give a contribution, which he calls the "saturation potential," to the single-particle potential energy $U(m)$ of occupied states. Diagram A1 has been evaluated for nuclear matter by Brueckner, Gammel, and Kubis[25] and by Köhler,[26] and for the nucleus O^{16} by McCarthy[27] and by Wong.[28] We will see later that it is one of the largest four-hole-line diagrams.

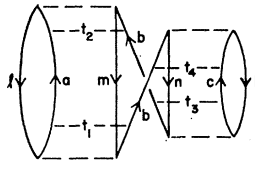

FIG. 7. Goldstone diagram to which GTO can be applied. Diagrams of this type are summed by means of GTO into the diagram of class A3.

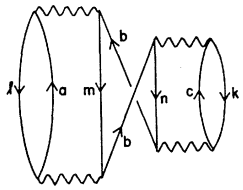

FIG. 8. Four-hole-line diagram of class A3.

The time restrictions (2.3) include all possibilities in Fig. 2 that have t_7 below both t_3 and t_6. New classes of diagrams are obtained if t_7 is allowed to lie above t_3 or t_6. All of these new diagrams contain bubble insertions into hole lines. They are exactly canceled by $U(m)$ and are therefore of only academic interest. So we shall not write them down.

Class A2. In order to analyze the structure shown in Fig. 5, we group the diagrams according to the relative order of t_3, t_6, t_9. All diagrams with $t_3>t_6>t_9$ are included by the time restrictions

$$t_1<t_6<t_2, \qquad t_4<t_9<t_5, \tag{2.5}$$

and their sum is the G-matrix diagram of Fig. 6(a). All diagrams with either $t_3>t_9>t_6$ or $t_9>t_3>t_6$ are included by the restrictions

$$t_7<t_6<t_8, \qquad t_1<t_6<t_2. \tag{2.6}$$

These diagrams are summed to give Fig. 6(b).

Class A2 consists of the two diagrams in Fig. 6. The contribution to the energy per particle from Fig. 6(a) is equal to

$$\begin{aligned} -A^{-1}\sum & \langle lm \mid G(lm)[Q/e(lm)] \mid ab\rangle \\ & \times\langle ab \mid [Q/e(lm)]G(lm) \mid lm-ml\rangle \\ & \times\langle kn \mid G(mj) \mid mj\rangle\langle mj \mid G(mj)[Q/e(mj)] \mid cd\rangle \\ & \times\langle cd \mid [Q/e(kn)]G(kn) \mid kn-nk\rangle. \end{aligned} \tag{2.7}$$

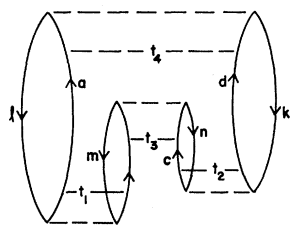

FIG. 9. Goldstone diagram to which GTO can be applied. Diagrams of this type are summed by means of GTO into the diagram of class A4.

[25] K. A. Brueckner, J. L. Gammel, and J. T. Kubis, Phys. Rev. **118**, 1438 (1960).
[26] H. S. Köhler, Nucl. Phys. **A128**, 273 (1968).
[27] R. J. McCarthy, Nucl. Phys. **A130**, 305 (1969).
[28] C. W. Wong, Nucl. Phys. **A104**, 417 (1967).

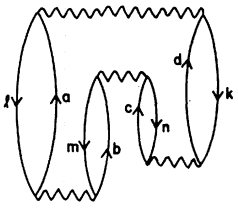

FIG. 10. Four-hole-line diagram of class A4.

The contribution from Fig. 6(b) is the same except that $\langle kn \mid G(mj) \mid mj \rangle$ is replaced by $\langle kn \mid G(kn) \mid mj \rangle$. Other relative time orders of t_3, t_6, t_9 lead to diagrams with bubble insertions into hole lines and will not be written down.

Class A3. Applying the time restrictions

$$t_1 < t_4 < t_2, \qquad t_3 < t_4 \tag{2.8}$$

to Fig. 7 gives the diagram shown in Fig. 8. This diagram, which constitutes class A3, gives the simplest on-energy-shell modification of the potential energy $U(b)$ of intermediate states. It has been discussed by Brandow,[5] and its contribution is

$$W(\text{A3}) = A^{-1} \sum \langle lm \mid G(lm)[Q/e(lm)] \mid ab \rangle U(b) \times \langle ab \mid [Q/e(lm)] G(lm) \mid lm - ml \rangle, \tag{2.9}$$

$$U(b) = \sum_{cnk} \langle nk \mid G(nk) \mid bc \rangle \langle bc \mid [Q/e(nk)] \times G(nk) \mid nk - kn \rangle. \tag{2.10}$$

Time orders different from (2.8) are permissible in Fig. 7—for example, we could have $t_1 > t_4$. However, all these new time orders lead to four-body cluster diagrams, which are discussed in Sec. II C.

Class A4. The diagrams of class A4 arise from the structure of Fig. 9 with the time restrictions

$$t_1 < t_3 < t_4, \qquad t_2 < t_3. \tag{2.11}$$

So class A4 contains the single G-matrix diagram shown in Fig. 10. Its contribution to the energy per particle is

$$W(\text{A4}) = -A^{-1}\tfrac{1}{2} \sum \langle lk - kl \mid G(kl)[Q/e(kl)] \mid ad \rangle \times \langle mn - nm \mid G(mn) \mid bc \rangle \times \langle cd \mid [Q/e(nk)] G(nk) \mid nk - kn \rangle \times \langle ab \mid [Q/e(lm)] G(lm) \mid lm - ml \rangle, \tag{2.12}$$

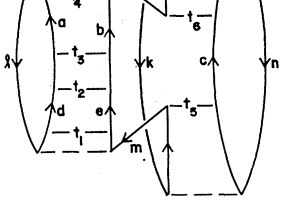

FIG. 11. Goldstone diagram to which GTO can be applied. Diagrams of this type are summed by means of GTO into the diagrams of class A5.

where the factor $\frac{1}{2}$ corrects for the fact that each distinct diagram is counted twice in the GTO treatment.

It might be thought that Fig. 10 is a four-body cluster diagram. However, we define the sum of the four-body clusters to be the "irreducible compact part with four external lines" of Brandow.[5] Therefore, in any four-body cluster diagram, there must occur (perhaps only inside a single G matrix) at least one energy denominator that involves the excitation of *four* particles above the Fermi sea. Figure 10 does not satisfy this requirement because the GTO has put all the G matrices and energy denominators on the energy shell. The decision about which diagrams are to be called four-body clusters is not completely arbitrary. The summation of four-body clusters leads to a four-body equation of Faddeev type (Sec. II C), and the simple form of this equation is spoiled if one tries to include Fig. 10.

Time orders different from (2.11) are possible in Fig. 9. But all such time orders lead to four-body cluster diagrams, which are considered in Sec. II C.

Class A5. The time restrictions

$$t_1 < t_5 < t_2, \qquad t_3 < t_6 < t_4 \tag{2.13}$$

in Fig. 11 lead to the diagram of Fig. 12, which forms class A5. Equation (2.13) covers all possibilities except for $t_5 > t_6$, which is included in the three-body combination class B3 (Sec. II B).

A new feature appears in Fig. 11. This diagram could be drawn with the interactions labeled t_2 and t_3 left out. It is these two interactions that form the ladder that is eventually summed to obtain the G matrix at the level of the arrow in Fig. 12. If they are left out, the corresponding G matrix does not appear in Fig. 12. Thus the arrow in Fig. 12 indicates an *optional* particle-particle interaction. Class A5 contains two distinct diagrams; in one, the optional particle-particle interaction is included, and in the other it is left out. From now on, a horizontal arrow, as in Fig. 12, will always imply an optional particle-particle interaction.

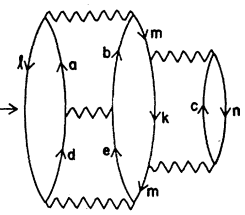

FIG. 12. Four-hole-line diagram of class A5.

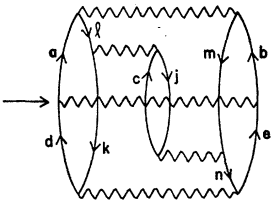

FIG. 13. Four-hole-line diagram of class A6.

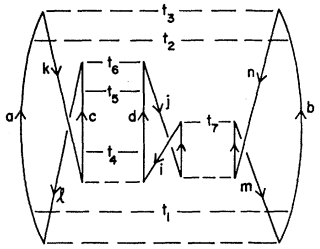

FIG. 14. Goldstone diagram to which GTO can be applied. Diagrams of this type are summed by means of GTO into the diagram of class A7.

The contribution from class A5 is

$$W(\mathrm{A5}) = -A^{-1}\sum \langle lm \mid G(lm)[Q/e(lm)] \mid ab\rangle \times\langle kn \mid G(kn) \mid mc\rangle(E_a+E_b+E_c-E_l-E_k-E_n)^{-1} \times\langle mc \mid G(kn) \mid kn-nk\rangle \times\{\langle ab \mid [Q/e(lm)]G(lm) \mid lm-ml\rangle - \sum_{de}\langle ab \mid G(lkn;c)[Q/e(lkn;c)] \mid de\rangle \times\langle de \mid [Q/e(lm)]G(lm) \mid lm-ml\rangle\}. \quad (2.14)$$

This diagram, without the optional particle-particle interaction, has been discussed previously in Refs. 5 and 25–27.

Class A6. The diagram of Fig. 13, which forms class A6, arises from a GTO treatment analogous to that of class A5. Its contribution to the energy per particle is similar to (2.14) and will not be written down.

Class A7. The diagrams arising from the structure of Fig. 14 can be classified according to the relative time order of t_3, t_6, t_7. For each of the six possible time orders, the GTO treatment sums a class of diagrams. However, because of the high degree of symmetry of Fig. 14, these six classes of diagrams are all identical, and only one of them must be counted. This is done by using the time restrictions

$$t_1<t_7<t_2, \qquad t_4<t_7<t_5 \quad (2.15)$$

and leads to the G-matrix diagram of class A7 shown in Fig. 15.

The restrictions (2.15) include all diagrams with either $t_3>t_6>t_7$, or $t_6>t_3>t_7$. Thus we have summed two identical classes of diagrams, and we must insert a factor $\frac{1}{2}$ into the contribution of class A7 to correct

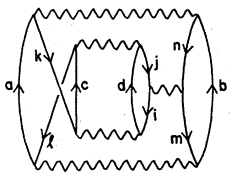

FIG. 15. Four-hole-line diagram of class A7.

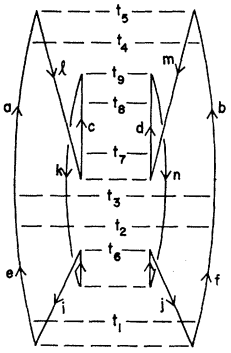

FIG. 16. Goldstone diagram to which GTO can be applied. Diagrams of this type are summed by means of GTO into the diagrams of classes A8 and A9.

or this. Thus we obtain

$$W(\mathrm{A7}) = -A^{-1}\tfrac{1}{2}\sum \langle kn \mid G(kn)[Q/e(kn)] \mid ab\rangle \langle ab \mid [Q/e(lm)]G(lm) \mid lm-ml\rangle \times\langle lj \mid G(lj)[Q/e(lj)] \mid cd\rangle \times\langle cd \mid [Q/e(ki)]G(ki) \mid ki-ik\rangle\langle im \mid G(jn) \mid jn-nj\rangle. \quad (2.16)$$

Class A8. The diagrams arising from Fig. 16 are grouped into six classes according to the relative time order of t_5, t_6, t_9. Only two of the six classes are distinct. We take these to be the class with $t_5>t_9>t_6$ and the class with $t_9>t_5>t_6$.

All diagrams with $t_5>t_9>t_6$ are included by the time restrictions

$$t_1<t_6<t_2, \qquad t_3<t_9<t_4. \quad (2.17)$$

These restrictions lead to the diagram of class A8 shown in Fig. 17. As usual, the horizontal arrow indicates an *optional* particle-particle interaction. The contribution from class A8 is

$$W(\mathrm{A8}) = -A^{-1}\tfrac{1}{2}\sum \langle lm \mid G(lm)[Q/e(lm)] \mid ab\rangle \times\langle kn \mid G(lm) \mid lm\rangle(E_a+E_b-E_k-E_n)^{-1} \times\langle ij \mid G(kn) \mid kn\rangle\{\langle ab \mid [Q/e(ij)]G(ij) \mid ij-ji\rangle - \sum_{ef}\langle ab \mid G(kn)[Q/e(kn)] \mid ef\rangle \times\langle ef \mid [Q/e(ij)]G(ij) \mid ij-ji\rangle\}. \quad (2.18)$$

Class A9. All diagrams that arise from Fig. 16 with $t_9>t_5>t_6$ are included by the restrictions

$$t_1<t_6<t_2, \qquad t_7<t_5<t_8. \quad (2.19)$$

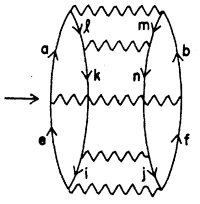

FIG. 17. Four-hole-line diagram of class A8.

The resulting G-matrix diagram of class A9 is shown in Fig. 18. Its contribution is

$$W(\mathrm{A9}) = A^{-1}\tfrac{1}{4}\sum \langle kn \mid G(kn)[Q/e(kn)] \mid cd\rangle \langle cd \mid [Q/e(lm)]G(lm) \mid lm-ml\rangle \times \langle lm \mid G(kn)[Q/e(kn)] \mid ef\rangle \times \langle ef \mid [Q/e(ij)]G(ij) \mid ij-ji\rangle\langle ij \mid G(kn) \mid kn\rangle. \quad (2.20)$$

One might have expected that the starting energy of the second interaction from the top in Fig. 18 would be E_l+E_m, but the GTO treatment gives E_k+E_n instead.

Additional diagrams. There are a number of two-body combination diagrams that have not yet been considered. However, all of them contain bubble insertions into *hole* lines and are therefore exactly canceled[4,8] by $U(m)$ in a self-consistent calculation. Some of these diagrams arise from new time orders in GTO structures that have already been written down, and some arise from completely new structures. Since these diagrams are of no practical interest, we shall not explicitly enumerate them.

In order to check that no diagrams have been overlooked, the terms in the nuclear-matter theory of Coester,[29] which is an algebraic formulation and does not involve diagrams, have been grouped according to number of independent hole lines. All two-body combination terms of the Coester theory are accounted for by diagrams. A similar check was made for the three-body combination diagrams and for the four-body clusters.

B. Three-Body Combination Diagrams

Three-body combination diagrams require the solution of the same three-body equation as the three-body cluster diagrams, but no four-body equations appear. We shall first review the treatment of the three-body clusters. This will fix our notation and remind the reader of some ideas that are useful for four-hole-line diagrams. Then we will write down the three-body combination diagrams and give formulas for their contributions.

A typical three-body cluster diagram ends at the top with the structure shown in Fig. 19(a) and begins at the bottom as in Fig. 19(b). In between there can be

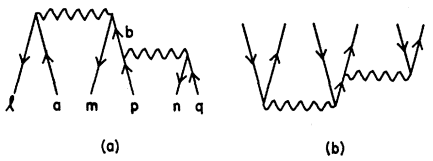

FIG. 19. Parts of a typical three-body-cluster diagram. Diagram (a) shows the last two interactions at the top, and (b) shows the first two interactions at the bottom.

0, 1, 2, ... particle-particle interactions. In addition, the diagrams of Figs. 1(a) and 1(b) are considered to be three-body cluster diagrams.

We must sum all topologically different diagrams of the type just described. Neglecting for the moment the diagrams of Figs. 1(a) and 1(b), we see that every diagram must end at the top as in Fig. 19(a). This structure topologically specifies all the particle and hole lines. For example, particle line a is the one that participates in the last interaction but not in the next-to-last interaction. Analogous statements can be made for p and q. The hole lines are topologically specified by being associated with specified particle lines, l with a, m with p, and n with q. As we work downward from Fig. 19(a), inserting more and more particle-particle interactions, particle line a may change its state many times. However, we shall mean by "line a" the entire length of this topologically specified particle line. Similar remarks apply to lines p and q.

Working downwards from Fig. 19(a), we can specify any three-body diagram by stating which pair of particle lines is involved in each successive interaction. There must be at least two interactions in addition to those of Fig. 19(a), and the last two at the bottom must have the appearance of Fig. 19(b). Because the particle lines are topologically specified by Fig. 19(a), including every possible sequence of interactions below Fig. 19(a) counts each topologically different diagram exactly once.[30]

In the first two interactions at the bottom of the diagram, the hole lines also participate. It is at this point, and *only* at this point,[13,14] that the question of exchange diagrams arises. There are three points at which hole lines can end in the bottom two interactions. The three topologically specified hole lines can be distributed among these three points in six ways. By definition, direct diagrams are those in which hole line l terminates with particle line a, m with p, and n with q. Thus each direct diagram has exactly three closed loops. Corresponding to each direct diagram are five exchange diagrams that are obtained by permuting the end points of the hole lines at the bottom of the diagram. This treatment of exchange is completely dif-

FIG. 18. Four-hole-line diagram of class A9.

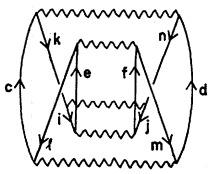

[29] F. Coester, in *Lectures in Theoretical Physics (Boulder, 1968)*, edited by K. T. Mahanthappa (Gordon and Breach, Science Publishers Inc., New York, 1969), Vol. XI.

[30] It is always understood that two successive G-matrix interactions between the same pair of particles do not occur. This would give a redundant ladder diagram, which is not permitted in the Brueckner-Goldstone expansion.

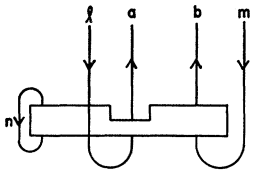

FIG. 20. Diagrammatic representation of expression (2.25) of the text.

ferent from the one used for two-body combination diagrams.

The contribution from all three-body clusters is the product of the two G-matrix elements of Fig. 19(a) times the appropriate amplitude for exciting three particles above the sea. This amplitude will contain sequences of two or more interactions that begin at the bottom as in Fig. 19(b). We also insert into this amplitude two terms of first order in G which, when combined with Fig. 19(a), will account for the diagrams of Figs. 1(a) and 1(b). The topmost interaction in this amplitude must not involve the pair (pq) because this would give a redundant ladder diagram when combined with Fig. 19(a). This amplitude is denoted by $\langle apq \mid Z_1 \mid lmn\rangle$ and satisfies the well-known Bethe-Faddeev equation[12–14]

$$\langle apq \mid Z_1 \mid lmn\rangle = \langle ap \mid [Q/e(lm)]G(lm) \mid lm\rangle\delta(q,n) + \langle aq \mid [Q/e(ln)]G(ln) \mid ln\rangle\delta(p,m) - \sum_{rs} \langle ap \mid [Q/e(lmn;q)]G(lmn;q) \mid rs\rangle\langle rsq \mid Z_3 \mid lmn\rangle - \sum_{rs} \langle aq \mid [Q/e(lmn;p)]G(lmn;p) \mid rs\rangle \times \langle rps \mid Z_2 \mid lmn\rangle, \quad (2.21)$$

with two similar equations for Z_2 and Z_3.

The subscript on Z_1 indicates that the first index a participates in the last interaction. The first two terms on the right-hand side of (2.21), when combined with Fig. 19(a), give the contribution of the diagrams of Figs. 1(a) and 1(b). All other three-body cluster diagrams are obtained by iterating Eq. (2.21) and the similar equations for Z_2 and Z_3. Only the terms of first order in G in formula (2.21) can have either p or q in the Fermi sea. All higher-order terms vanish unless p and q are both above the sea.

After the Bethe-Faddeev equations have been solved for Z_1, the contribution from Fig. 19(a) is combined with Z_1 to obtain the energy per particle W_3 from all three-body cluster diagrams in the form

$$W_3 = A^{-1}\sum_{lmn} W_3(lmn), \quad (2.22)$$

$$W_3(lmn) = \sum_{pqab} \langle lm \mid G(lm)[Q/e(lm)] \mid ab\rangle \times \langle bn \mid G(lmn;a) \mid pq\rangle\langle apq \mid Z_1 \mid lmn\rangle. \quad (2.23)$$

In all diagrams generated by (2.23) particle line a and hole line l form a closed loop, and so do (p, m) and (q, n). Thus (2.23) includes only the direct diagrams. How can the exchange diagrams be included? Permuting hole lines l and m at the bottom of a direct diagram corresponds to replacing $\langle apq \mid Z_1 \mid lmn\rangle$ by $\langle apq \mid Z_1 \mid mln\rangle$. There is also an additional minus sign because permuting l and m changes the number of closed loops in the three-body diagram by one. Pursuing this argument, one finds that all exchange diagrams are included by replacing Z_1 by Z_1^A, where

$$\langle apq \mid Z_1^A \mid lmn\rangle = \sum_P (-1)^P \langle apq \mid Z_1 \mid P(lmn)\rangle. \quad (2.24)$$

The sum is over all permutations P of the indices (lmn). Thus all three-body cluster diagrams, both direct and exchange, are given by formula (2.23) with Z_1 replaced by Z_1^A.

The sign of (2.23) is given by $(-1)^{h+l+e}$. In a direct three-body cluster diagram there are three hole lines and three closed loops. Thus $(-1)^{h+l}=+1$, and we have only to consider $(-1)^e$. By iterating (2.21) we see that every term in Z_1 has one more energy denominator than it has factors of (-1). So one factor of e is always left over in Z_1. The resulting minus sign is canceled in (2.23) by a further minus sign that comes from the energy denominator in $\langle lm \mid G(Q/e) \mid ab\rangle$. So the final result is a plus sign for expression (2.23).

In order to draw the three-body combination diagrams, we introduce a diagrammatic representation for certain three-body amplitudes. Our representation is similar to the compact-cluster diagrams of Brandow,[5] but there are differences of detail. The quantity

$$\sum_{pq} \langle bn \mid G(lmn;a) \mid pq\rangle\langle apq \mid Z_1 \mid lmn\rangle \quad (2.25)$$

is represented by the diagram of Fig. 20. The fact that line a emerges from a notch in the three-body block indicates that a did not participate in the last interaction. This notch could appear at either end of the three-body block as well as in the middle, and so could the closed loop labeled n. Formula (2.25) contains Z_1, not Z_1^A, so that line a is topologically associated with line l, and similarly for b and m.

Another useful amplitude, denoted by $\langle abc \mid Y \mid lmn\rangle$, is given by the sum of all three-body diagrams, of second or higher order in G, that produce particles a, b, c and holes l, m, n, with a and l originating at the same point and similarly for (b, m) and (c, n). All second-order diagrams in Y have the topology of Fig. 19(b), and higher-order diagrams are obtained by inserting additional particle-particle interactions. We

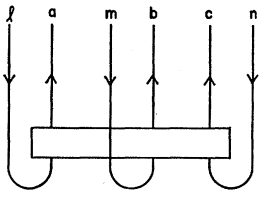

FIG. 21. Diagrammatic representation of $\langle abc|Y|lmn\rangle$.

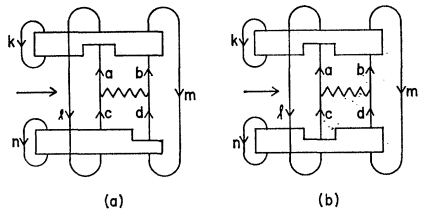

FIG. 22. Four-hole-line diagrams of class B1.

can obtain Y by subtracting out the first-order terms from the Z_i to get

$$\langle pqr \mid Y \mid lmn\rangle = -\tfrac{1}{2}\langle pqr \mid Z_1+Z_2+Z_3 \mid lmn\rangle + \langle pq \mid [Q/e(lm)]G(lm) \mid lm\rangle\delta(r,n) + \langle pr \mid [Q/e(ln)]G(ln) \mid ln\rangle\delta(q,m) + \langle qr \mid [Q/e(mn)]G(mn) \mid mn\rangle\delta(p,l). \quad (2.26)$$

This expression vanishes unless p, q, and r are all above the Fermi sea.

The diagrammatic representation of $\langle abc \mid Y \mid lmn\rangle$ is shown in Fig. 21. The left-right order of the lines a, b, c is immaterial, as long as a is associated with l, b with m, and c with n. The quantity Y^A is defined in analogy with Eq. (2.24) for $Z_1{}^A$.

The over-all sign for a three-body combination diagram is obtained by evaluating $(-1)^{h+l+e}$ for a direct diagram. The minus signs introduced by exchange diagrams are always taken into account by using antisymmetrized matrix elements. The value of $(-1)^{h+l}$ is always obvious from the topology of the diagram. To calculate $(-1)^e$, note that Z_i has one energy denominator "left over" without an accompanying minus sign but that Y does not. Thus the value of $(-1)^e$ is obtained from the formula for the contribution of any diagram by including a factor -1 for each factor Z_i and for each energy denominator that appears explicitly in the formula. These rules have already been used to obtain the over-all sign for expression (2.23). We shall use them without further comment in writing formulas for the three-body combination diagrams.

This completes our review of the three-body cluster diagrams. The ideas and notation that have been developed will now be used to write formulas for the three-body combination diagrams.

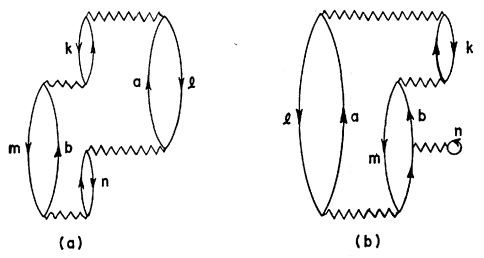

FIG. 23. Two diagrams of fourth order in G that are contained in class B1.

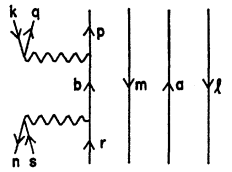

FIG. 24. Part of a typical diagram of class B1 that is used to specify the particle and hole lines topologically.

Class B1. Class B1 consists of the diagrams in Fig. 22(a) and 22(b). In these diagrams there is no opportunity to use the GTO treatment. Two of the simplest diagrams belonging to class B1 are shown in Fig. 23. In these diagrams, the excitation of three particles above the Fermi sea occurs only *inside* certain G matrices. Diagrams of greater than fourth order in G will have three particles excited above the sea at one or more points *between* G matrices.

To see what the contribution from class B1 is, we consider Fig. 22(b) without the optional particle-particle interaction. The lowest interaction in the upper three-body block and the topmost interaction in the lower three-body block are shown in Fig. 24. These two interactions topologically specify all the particle and hole lines shown in Fig. 24, except that there is no distinction between the hole lines l and m. Therefore, working either upward or downward from Fig. 24, each different sequence of two-body interactions leads to a distinct direct diagram. So we obtain the amplitude Z_1 at both the top and bottom, as indicated in Fig. 22. Permutations of the end points of hole lines at either the top or bottom of Fig. 22 are included by using $Z_1{}^A$ instead of Z_1. However, since Fig. 24 does not distinguish between l and m, the permutation of l and m in *both* the top and bottom of Fig. 22 leaves the topology of the diagram unchanged. A factor $\frac{1}{2}$ is needed to correct for this double counting. So the contribution from class B1 is found to be

$$W(\mathrm{B1}) = -A^{-1}\tfrac{1}{2}\sum \langle lmk \mid Z_1{}^{\dagger A} \mid apq\rangle \times \langle pq \mid G(lmk;a) \mid bk\rangle(E_a+E_b-E_l-E_m)^{-1} \times \{\langle an \mid G(lmn;b) \mid rs\rangle\langle rbs \mid Z_2{}^A \mid lmn\rangle + \langle bn \mid G(lmn;a) \mid rs\rangle\langle ars \mid Z_1{}^A \mid lmn\rangle - \langle ab \mid G(lm)[Q/e(lm)] \mid cd\rangle[\langle cn \mid G(lmn;d) \mid rs\rangle \times \langle rds \mid Z_2{}^A \mid lmn\rangle + \langle dn \mid G(lmn;c) \mid rs\rangle \times \langle crs \mid Z_1{}^A \mid lmn\rangle]\}. \quad (2.27)$$

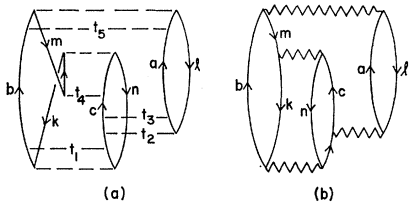

FIG. 25. An illustration of the GTO treatment that leads to diagrams of class B2. Applying GTO to diagram (a) gives diagram (b), which is a typical member of class B2.

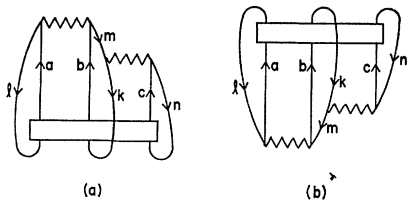

FIG. 26. Four-hole-line diagrams of class B2.

The first two terms inside the curly brackets of (2.27) come from Figs. 22(a) and 22(b), respectively, with the optional particle-particle interaction omitted. The last two terms inside the curly brackets take account of the optional particle-particle interaction.

Class B2. Applying the GTO to Fig. 25(a), we find that the time restrictions

$$t_1<t_2, \qquad t_3<t_4<t_5 \tag{2.28}$$

lead to the diagram of Fig. 25(b). The GTO puts the next-to-top G matrix on the energy shell in Fig. 25(b). Thus no energy denominator involves more than three particles above the sea, and Fig. 25(b) is therefore not a four-body cluster diagram. Taking $t_4<t_3$ in Fig. 25(a) *does* lead to a four-body cluster diagram.

Figure 25(b) shows one member of the class B2. In a typical diagram of this class, three particles are excited above the sea and interact among themselves any number of times. Then the diagram ends at the top with two interactions like those of Fig. 25(b). All members of class B2 are represented by the diagrams of Fig. 26.

To write the contribution from Fig. 26(a), note that the top two interactions topologically specify all the particle and hole lines. The topmost interaction of the three-body block is not restricted by the requirement that redundant ladder diagrams be omitted. Thus the correct three-body amplitude is Y, as is already indicated in Fig. 26. Permutations of the hole lines lkn at the bottom of the diagram are included by using the antisymmetrized Y^A. The total contribution from class

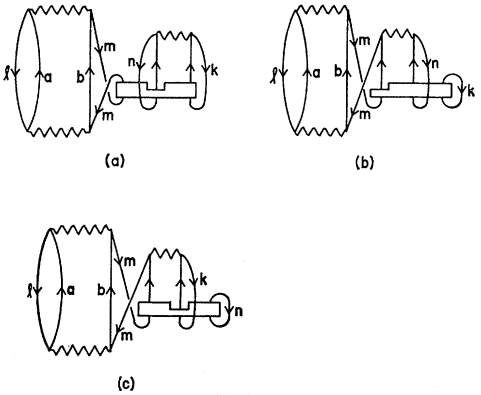

FIG. 27. Four-hole-line diagrams of class B3.

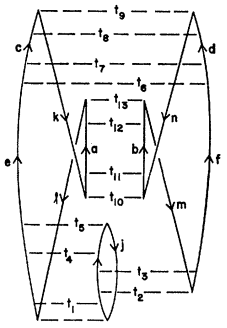

FIG. 28. Goldstone diagram to which GTO can be applied. Diagrams of this type are summed by means of GTO into the diagrams of classes B4, B5, and B6.

B2 is then

$$W(\mathrm{B2})=A^{-1}2\sum\langle lm\mid G(lm)[Q/e(lm)]\mid ab\rangle \times\langle kn\mid G(kn)\mid mc\rangle\langle abc\mid Y^A\mid lkn\rangle. \tag{2.29}$$

We have inserted a factor of 2 to take account of Fig. 26(b), whose contribution is equal to that of Fig. 26(a).

Class B3. The diagrams of class B3 are shown in Fig. 27. Each diagram has a three-body cluster inserted into the hole line of a two-body ladder. Thus these diagrams can be taken into account by a modification of the single-particle potential $U(m)$.[5] A simple application of the GTO puts each three-body cluster completely on the energy shell.

To obtain the contribution from class B3, note that all particle and hole lines are topologically specified by the top two interactions of the three-body insertion and the lower interaction of the two-body ladder. Thus Z_1 is the correct amplitude to use in the three-body insertion. Permutation of m, k, and n at the bottom of the three-body insertion replaces Z_1 by $Z_1{}^A$. Permutation of l and m at the top of the two-body ladder gives a direct-minus-exchange matrix element of G at this point. So we find

$$W(\mathrm{B3})=-A^{-1}\sum\langle lm-ml\mid G(lm)[Q/e(lm)]\mid ab\rangle \times\langle ab\mid[Q/e(lm)]G(lm)\mid lm\rangle \times[W_3{}^A(nkm)+W_3{}^A(mnk)+W_3{}^A(kmn)], \tag{2.30}$$

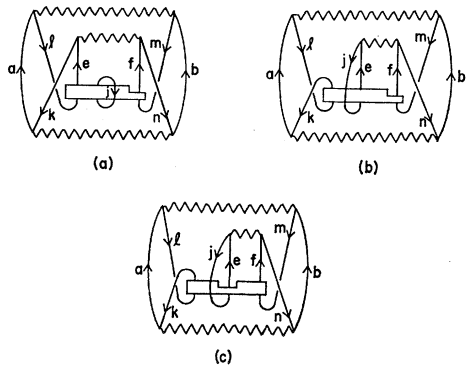

FIG. 29. Four-hole-line diagrams of class B4.

where $W_3^A(lmn)$ is defined by (2.23) with Z_1^A instead of Z_1.

Class B4. In Fig. 28 the interactions $t_1 \cdots t_9$ form a three-body cluster diagram with two of its hole lines broken open and the two-body ladder $t_{10} \cdots t_{13}$ inserted therein. In applying the GTO we group the diagrams according to the position of t_{13} relative to $t_1, \ldots, t_9$. A change of ordering among $t_1, \ldots, t_9$ gives a diagram with a different three-body cluster part. Since we will eventually include all possible three-body cluster parts, this gives nothing new. So the ordering among $t_1, \ldots, t_9$ can be kept fixed.

All diagrams with $t_{13} > t_9$ are included by the restrictions

$$t_{11} < t_9 < t_{12}. \tag{2.31}$$

This gives a G-matrix diagram of the type shown in Fig. 29(a). Distinct diagrams of the same type are obtained by breaking open topologically different pairs of hole lines in a given three-body part. This gives the diagrams of Figs. 29(b) and 29(c) which, together with Fig. 29(a), make up class B4.

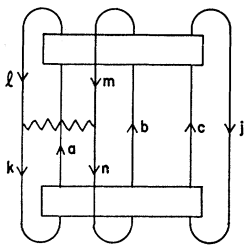

FIG. 30. Four-hole-line diagrams of class B5.

In any diagram of class B4, all particle and hole lines are topologically specified by the top two interactions in the three-body part. All exchange diagrams are included by permuting the hole lines ljm at the bottom of the three-body block. So the contribution to the energy per particle from class B4 is

$$\begin{aligned} W(\mathrm{B4}) = A^{-1} \sum & \langle lm \mid G(lm)[Q/e(lm)] \mid ab\rangle\langle ab \mid [Q/e(kn)]G(kn) \mid kn\rangle[\langle kn \mid G(lm)[Q/e(lm)] \mid ef\rangle \\ & \times \langle ej \mid G(lmj;f) \mid pq\rangle\langle fpq \mid Z_1^A \mid mlj\rangle + \langle jn \mid G(jn)[Q/e(jn)] \mid ef\rangle\langle ek \mid G(lmj;f) \mid pq\rangle \\ & \times \langle fpq \mid Z_1^A \mid mjl\rangle + \langle jn \mid G(jn)[Q/e(jn)] \mid ef\rangle\langle kf \mid G(lmj;e) \mid pq\rangle\langle epq \mid Z_1^A \mid jlm\rangle]. \end{aligned} \tag{2.32}$$

The value of the starting energy in the second interaction from the top in Fig. 29(a) is unexpected but follows directly from the GTO treatment.

Class B5. Suppose in Fig. 28 that t_{13} lies between t_2 and t_5, i.e., at a level where three particles are excited above the Fermi sea. Then all interactions below t_{13} will be combined into a three-body cluster part that produces three particle-hole pairs, and all interactions above t_{13} will be combined into a second three-body part. The resulting diagrams of class B5 are represented by Fig. 30. The GTO simply puts the hole-hole interaction on the energy shell.

To obtain the contribution from class B5, note first that the hole-hole interaction topologically specifies the hole lines l, m, and j except that it does not distinguish between l and m. We can take the hole lines to be completely specified and correct later for the ambiguity between l and m by inserting a factor of $\frac{1}{2}$. The particle lines are then topologically specified by terminating at the top of the diagram with specified hole lines. Subject to this last requirement, every sequence of interactions above the hole-hole interaction is possible and gives a distinct diagram. Thus the upper three-body block gives $\langle lmj \mid Y^\dagger \mid abc\rangle$. Since all particle and hole lines are now topologically specified, every sequence of interactions below the hole-hole interaction must be included. This gives a factor $\langle abc \mid Y \mid knj\rangle$. The question of exchange arises only in terminating the hole lines at the bottom of the diagram. Thus we get

$$\begin{aligned} W(\mathrm{B5}) = A^{-1}\tfrac{1}{2} \sum & \langle lmj \mid Y^\dagger \mid abc\rangle \\ & \times \langle kn \mid G(lm) \mid lm\rangle\langle abc \mid Y^A \mid knj\rangle. \end{aligned} \tag{2.33}$$

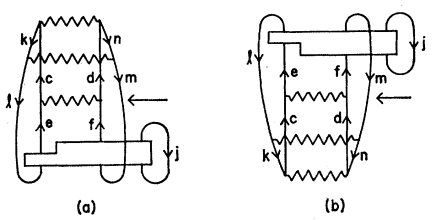

FIG. 31. Four-hole-line diagrams of class B6.

Class B6. The final class of diagrams obtainable from Fig. 28 comes from time orders with $t_5 < t_{13} < t_9$. All such diagrams are included by the restrictions

$$t_1 < t_{13} < t_8. \tag{2.34}$$

All diagrams of this type are represented by Fig. 31(a), which, along with the similar diagrams represented by Fig. 31(b), make up class B6.

The particle and hole lines in Fig. 31(a) are topologically specified in the same way as they are in a three-body cluster diagram. The contribution of Fig. 31(a) is

$$\begin{aligned} -A^{-1} \sum & \langle kn \mid G(kn)[Q/e(kn)] \mid cd\rangle\langle lm \mid G(kn) \mid kn\rangle \\ & \times (E_c + E_d - E_l - E_m)^{-1}[\langle dj \mid G(lmj;c) \mid pq\rangle \\ & \times \langle cpq \mid Z_1^A \mid lmj\rangle - \langle cd \mid G(lm)[Q/e(lm)] \mid ef\rangle \\ & \times \langle fj \mid G(lmj;e) \mid pq\rangle\langle epq \mid Z_1^A \mid lmj\rangle]. \end{aligned} \tag{2.35}$$

The contribution from Fig. 31(b) is given by the same expression except that $\langle lm \mid G(kn) \mid kn\rangle$ is replaced by $\langle lm \mid G(lm) \mid kn\rangle$.

Other classes. All additional classes of three-body

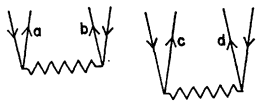

FIG. 32. One of the two possible ways of starting a four-body-cluster diagram. The other way is shown in Fig. 19(b).

combination diagrams that we have been able to find contain bubble insertions into hole lines. They are canceled by $U(m)$ and will not be written down.

C. Four-Body Cluster Diagrams

In a typical four-body cluster diagram, four particles are excited above the Fermi sea, interact any number of times, and finally fall back into the sea again. The sum of all four-body clusters gives Brandow's irreducible compact part with four external lines.[5] The distinguishing feature of these diagrams is that each one contains somewhere, possibly only *inside* a single G matrix, an energy denominator involving the excitation of four particles above the Fermi sea. This is not true of any two- or three-body combination diagram, either because at no point are four particles excited above the Fermi sea, or because of modification of the energy denominators by GTO.

Four particles can be excited above the Fermi sea in two quite different ways. If the first two interactions are as shown in Fig. 19(b), then the three excited particles can interact among themselves any number of times before a fourth particle is excited. If the first two interactions are as shown in Fig. 32, then we can have an alternating sequence of interactions cd, ab, cd, ab, ..., after which one of the pair a, b must interact with one of the pair c, d. After interacting among themselves any number of times, the four particles can be deexcited in two different ways that are analogous to the two different types of excitation.

If the diagram begins as in Fig. 19(b), then the first interaction involving a fourth particle will usually be as shown in Fig. 33(a). But it *may* instead be as shown in Figs. 33(b) or 33(c). In this latter case we have four particles above the Fermi sea only *inside* the v-matrix ladder that gives the G matrix of Figs. 33(b) or 33(c).

Having described the diagrams to be summed, we proceed to derive a formula for their contribution. The first step is to specify topologically the particle and hole lines by means of the interactions that deexcite the particles at the top of the diagram. As we have pointed out above, there are two different ways of deexciting the four particles. The first way is shown in

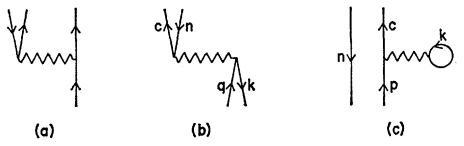

FIG. 33. Possibilities for the first interaction in a four-body-cluster diagram that involves a fourth particle. The diagram is assumed to have started as in Fig. 19(b).

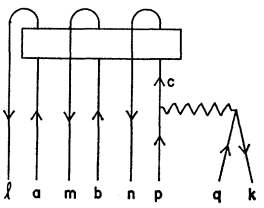

FIG. 34. Diagrammatic representation of the first of two ways of deexciting the particles in a four-body-cluster diagram.

Fig. 34. The lowest interaction in Fig. 34 topologically specifies the particle lines p and q. [If only three particles are excited below the level of Fig. 34, then the lowest interaction of Fig. 34 must be replaced by Figs. 33(b) or 33(c). In Fig. 33(b), we have $p=n$. In Fig. 33(c), we have $q=k$.] Particle lines a and b are specified as the remaining two particle lines, but this does not distinguish between a and b. We shall proceed as if all the particle lines were topologically specified and insert a factor of $\frac{1}{2}$ because of the ambiguity between a and b. The hole lines are topologically specified by terminating with specified particle lines at the top of the diagram. Having specified the particle lines by the G-matrix interaction of Fig. 34, we obtain a distinct diagram from every sequence of interactions above this G matrix. Thus the contribution from Fig. 34 is

$$\tfrac{1}{2}\langle lmn \mid V^{\dagger} \mid abc\rangle\langle ck \mid G(lmnk; ab) \mid pq\rangle. \quad (2.36)$$

The second way of deexciting the particles is shown in Fig. 35(a). The lowest interaction specifies which pair of particle lies are p and q but does not distinguish between p and q. This ambiguity will be corrected for by a factor of $\frac{1}{2}$. Assuming p and q to be specified topologically, we see that a and b are topologically specified by the upper two interactions of Fig. 35(a). The hole lines are then topologically specified by termininating with specified particle lines.

If only three particles are excited below the level of Fig. 35(a), then this figure must be replaced by Fig. 35(b), in which $p=n$, or by a similar diagram in which $q=k$. In Fig. 35(b) there is no ambiguity between p and q. But a factor of $\frac{1}{2}$ is still necessary because our formulas will include not only Fig. 35(b), but also the corresponding diagram with $q=k$, and these two diagrams are topologically identical (more precisely, they

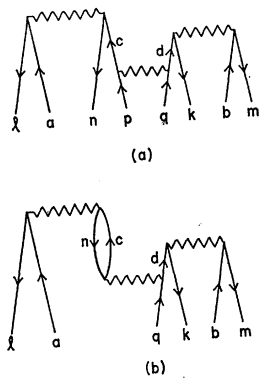

FIG. 35. Diagrammatic representation of the second of two ways of deexciting the particles in a four-body-cluster diagram. The difference between (a) and (b) is explained in the text.

become topologically identical after application of the GTO, which is described in the next paragraph).

We have drawn only two interactions above the lowest G matrix in Fig. 35. But there could be any alternating sequence of interactions ac, bd, ac, bd, ... All these possibilities are summed immediately by using the GTO. The result is simply to put the upper two G matrices and energy denominators of Fig. 35 on the energy shell. The factor associated with Fig. 35 is therefore

$$\tfrac{1}{2}\langle ln \mid G(ln)[Q/e(ln)] \mid ac\rangle \times\langle mk \mid G(mk)[Q/e(mk)] \mid bd\rangle \times\langle cd \mid G(lmnk; ab) \mid pq\rangle. \quad (2.37)$$

Let us now consider that part of a four-body cluster diagram that lies below Figs. 34 or 35. Since the particle lines are topologically specified, a distinct diagram is obtained from every sequence of interactions that takes particles from states l, m, n, and k in the Fermi sea to states a, b, p, and q. Either p or q (but not both) may be in the Fermi sea. Direct diagrams are defined to be those in which each hole line begins and ends with the same particle line. We will derive a formula for direct diagrams and include the exchange diagrams later.

We must calculate the appropriate amplitude $\langle abpq \mid C_{34} \mid lmnk\rangle$ for taking four particles from l, m, n, and k to a, b, p, and q. The subscript 34 means that the last interaction must *not* be between p and q, i.e., it must involve at least one of a, b. This requirement is necessary in order to avoid a redundant ladder diagram when C_{34} is combined with Figs. 34 or 35. The contribution to $\langle abpq \mid C_{34} \mid lmnk\rangle$ of all diagrams that excite three particles and leave the fourth particle in the sea is

$$\langle abp \mid Y \mid lmn\rangle\delta(q, k)+\langle abq \mid Y \mid lmk\rangle\delta(p, n). \quad (2.38)$$

Sequences of alternate interactions between two different pairs of particles (see Fig. 32) give, after application of GTO,

$$\langle ap \mid [Q/e(ln)]G(ln) \mid ln\rangle\langle bq \mid [Q/e(mk)]G(mk) \mid mk\rangle + \langle aq \mid [Q/e(lk)]G(lk) \mid lk\rangle \times\langle bp \mid [Q/e(mn)]G(mn) \mid mn\rangle. \quad (2.39)$$

All additional contributions to $\langle abpq \mid C_{34} \mid lmnk\rangle$ are grouped into five classes, according to which pair of a, b, p, and q (other than pq) participates in the last interaction. In this way we obtain the following equation for C_{34}:

$$\langle abpq \mid C_{34} \mid lmnk\rangle=\langle abp \mid Y \mid lmn\rangle\delta(q, k)+\langle abq \mid Y \mid lmk\rangle\delta(p, n)+\langle ap \mid [Q/e(ln)]G(ln) \mid ln\rangle \times\langle bq \mid [Q/e(mk)]G(mk) \mid mk\rangle+\langle aq \mid [Q/e(lk)]G(lk) \mid lk\rangle\langle bp \mid [Q/e(mn)]G(mn) \mid mn\rangle - \sum_{rs}\langle ab \mid [Q/e(lmnk; pq)]G(lmnk; pq) \mid rs\rangle\langle rspq \mid C_{12} \mid lmnk\rangle - \sum_{rs}\langle ap \mid [Q/e(lmnk; bq)]G(lmnk; bq) \mid rs\rangle\langle rbsq \mid C_{13} \mid lmnk\rangle+3 \text{ similar terms}. \quad (2.40)$$

There are five similar equations for the other five amplitudes C_{ij}. These six coupled equations are the four-body analog of the three-body Bethe-Faddeev equations (2.21). So the equations represented by (2.40) will be called the four-body Bethe-Faddeev equations.

The contribution to the energy from all four-body cluster diagrams is obtained by combining $\langle abpq \mid C_{34} \mid lmnk\rangle$ with the sum of (2.36) and (2.37). All exchange diagrams are obtained by permuting the hole lines at the bottom of the diagram. This corresponds to replacing C_{34} by $C_{34}{}^{A}$, which is defined in analogy with (2.24). The energy per particle from all four-body cluster diagrams is therefore given by

$$W_4=A^{-1}\tfrac{1}{2}\sum\{\langle lmn \mid Y^{\dagger} \mid abc\rangle\delta(r, k) +\langle ln \mid G(ln)[Q/e(ln)] \mid ac\rangle \times\langle mk \mid G(mk)[Q/e(mk)] \mid br\rangle\} \times\langle cr \mid G(lmnk; ab) \mid pq\rangle \times\langle abpq \mid C_{34}{}^{A} \mid lmnk\rangle. \quad (2.41)$$

To evaluate W_4, one must first solve the three-body Bethe-Faddeev equations to obtain Y. Then the four-body Bethe-Faddeev equations are solved for C_{34}, and the calculated values of C_{34} and Y are put into (2.41).

Formulas for four-body cluster diagrams have been given by Lawson and Sampanthar[31] and by Kuriyama.[32] The formalism developed in the present paper differs somewhat from both of these earlier treatments.

Lawson and Sampanthar define a four-body wave function $\phi-\psi^{(34)}$ that contains *all* diagrams of first or higher order with the last interaction *not* between particles 3 and 4. This wave function contains our C_{34} and a great many additional terms. For example, it contains all sequences of interactions among particles 1, 3, and 4 in which the last interaction is not between 3 and 4, and in which particle 2 remains undisturbed in the Fermi sea. These terms do not appear in C_{34}. Lawson and Sampanthar also use a slightly different

[31] P. A. Lawson and S. Sampanthar, Nucl. Phys. **A106**, 669 (1968).
[32] A. Kuriyama, Progr. Theoret. Phys. (Kyoto) **40**, 301 (1968).

definition of four-body clusters. For example, they include our class A4 among the four-body clusters.

Our formulation seems to have several advantages over that of Lawson and Sampanthar. First, our use of GTO in connection with Fig. 35 and Eqs. (2.37) and (2.39) makes our treatment simpler than theirs. Second, Lawson and Sampanthar's equation (24) for the energy, although formally exact, might produce some unnecessary error in a numerical calculation. In this equation, the contribution from terms of $\phi-\psi^{(34)}$ in which either particle 1 or particle 2 remains in the Fermi sea is identically zero. However, when these terms are explicitly evaluated in a practical calculation, in which approximations must always be made, they will usually turn out to be nonzero and thus produce some error. The wave function C_{34} used in the present formalism contains no "superfluous terms" of this sort. Third, our formal expressions are more explicit with respect to starting energies and exchange diagrams than those of Lawson and Sampanthar.

Kuriyama[32] defines a four-body wave function $\psi_{34}^{(c)}$ which consists of all *connected* diagrams of third or higher order in which the last interaction must involve particles 3 and 4 and no other pair. This wave function is clearly quite different from our C_{34} and from Lawson and Sampanthar's $\phi-\psi^{(34)}$. Kuriyama defines the Pauli operator Q_{ij} to require that *at least one* of the particles i, j be above the Fermi sea. The usual definition of Q_{ij}, which is used in the present work, requires *both* particles i and j to be above the sea. Kuriyama's use of a different Q allows many summations that would ordinarily run only over particle states to run over hole states as well. Hence many terms are included that do not correspond to diagrams in the Brueckner-Goldstone expansion. This is certainly undesirable, but in a practical calculation it might introduce only a small error. A more serious consequence of Kuriyama's definition of Q is that his formula (2-9) for W_4 excludes all diagrams that end at the top as in our Fig. 35. Therefore, it is believed that the formulation given in the present paper is preferable.

III. NUMERICAL CALCULATIONS

A. Preliminary Remarks

Before estimating the contributions from specific diagrams, we state some of the ideas, assumptions, and notation that will be used in making such estimates. All numerical work is done with the Reid[18] soft-core potential at normal density ($k_F=1.36$ F^{-1}). The single-particle energy spectrum is taken to be

$$E(k)=\tfrac{1}{2}k^2 \qquad k>k_F$$
$$=(1/2m^*)k^2+A_1, \qquad k<k_F \tag{3.1}$$
$$m^*=0.6, \qquad A_1=-81 \text{ MeV}. \tag{3.2}$$

We use units in which $(\hbar^2/M)=1$, where M is the nucleon mass. Then 1 F^{-2} is equivalent to 41.47 MeV. The choice of pure kinetic energy for intermediate-state energies is a sensible one in a scheme where three-body cluster diagrams are to be calculated explicitly.[4]

The spectrum (3.1) gives

$$\bar{U}=-66 \text{ MeV}, \tag{3.3}$$

where $\bar{U}$ is the average single-particle potential energy for occupied states. A detailed calculation[6] using this spectrum as input gave an output $\bar{U}$ of -65 MeV. The value $m^*=0.6$ agrees well with self-consistent values obtained by Sprung.[33] Thus our spectrum below the Fermi sea is very nearly self-consistent. Any inaccuracies due to lack of self-consistency will be negligible.

All the required two-body wave functions and matrix elements of G are calculated by a method invented by Kallio.[6] The only approximation in this method is the use of the angle-averaged Pauli operator,[10] which produces only very small errors.[34,35] Using the notation of Ref. 6, we define

$$\phi=\exp(i\mathbf{k}_0\cdot\mathbf{r})\chi_{m_S}^S, \tag{3.4}$$

$$\zeta=\phi-\psi, \tag{3.5}$$

where ϕ is the unperturbed two-body wave function, ψ is the correlated Bethe-Goldstone wave function, and ζ is the "defect function." The partial-wave expansion for ψ is

$$\psi(\mathbf{k}_0,\mathbf{r})=\sum_{JLL'} i^L[4\pi(2L+1)]^{1/2}$$
$$\times(LS0m_S\,|\,Jm_S)r^{-1}u_{LL'}{}^{JS}(k_0,r)\mathcal{Y}_{JLL'}{}^{m_S}(\hat{k}_0,\hat{r}), \tag{3.6}$$

where m_S is defined relative to the polar axis $\mathbf{k}_0$. Here $u_{LL'}{}^{JS}$ is the correlated wave in channel L' due to the unperturbed wave in the entrance channel L. In singlet states, and in triplet states with $J=L$, only $L'=L$ is possible. But, because of the tensor force, in triplet states with $L=J-1$, we can have $L'=L$ or $L+2$, and when $L=J+1$ we can have $L'=L$ or $L-2$. The partial-wave expansions of ϕ and ζ are the same as (3.6) except that $u_{LL'}{}^{JS}$ is replaced by $\delta(L,L')rj_L(k_0r)$ and by $\chi_{LL'}{}^{JS}=\delta(L,L')rj_L(k_0r)-u_{LL'}{}^{JS}$, respectively.

Using $G\phi=v\psi$, one obtains for matrix elements of G the result[6] (m_S and m_S' are *both* defined relative to the

[33] D. W. Sprung (private communication).
[34] G. E. Brown, G. T. Schappert, and C. W. Wong, Nucl. Phys. **56**, 191 (1964).
[35] E. J. Irwin, Ph.D. thesis, Cornell University, 1963 (unpublished).

polar axis $\mathbf{k}_0$)

$$\langle \mathbf{k}Sm_S' \mid G \mid \mathbf{k}_0Sm_S\rangle = \sum_{JLL'} i^{L-L'}[4\pi(2L+1)]^{1/2} \times (L'Sm_S - m_S'm_S' \mid Jm_S) \times (LS0m_S \mid Jm_S)\, Y_{L'm_S-m_S'}(\hat{k}, \hat{k}_0) G_{LL'}{}^{JS}(k, k_0), \quad (3.7)$$

$$G_{LL'}{}^{JS}(k, k_0) = 4\pi \sum_{L''} \int_0^\infty r j_{L'}(kr) \times \langle JL'S \mid v(r) \mid JL''S\rangle u_{LL''}{}^{JS}(k_0, r)\, dr. \quad (3.8)$$

The Fourier transform of ζ will also be needed. It is given by

$$\langle \mathbf{k}Sm_S' \mid \zeta(\mathbf{k}_0, S, m_S)\rangle = \sum_{JLL'} i^{L-L'}[4\pi(2L+1)]^{1/2} \times (L'Sm_S - m_S'm_S' \mid Jm_S) \times (LS0m_S \mid Jm_S)\, Y_{L'm_S-m_S'}(\hat{k}, \hat{k}_0) \chi_{LL'}{}^{JS}(k, k_0), \quad (3.9)$$

$$\chi_{LL'}{}^{JS}(k, k_0) = 4\pi \int_0^\infty r j_{L'}(kr) \chi_{LL'}{}^{JS}(k_0, r)\, dr. \quad (3.10)$$

Here, m_S and m_S' are both defined relative to $\mathbf{k}_0$. By using the relation[4] $\zeta = (Q/e)G\phi$, one can show that

$$\chi_{LL'}{}^{JS}(k, k_0) = [Q(k, K)/(k^2+\gamma^2)] G_{LL'}{}^{JS}(k, k_0), \quad (3.11)$$

where K is the total momentum of the interacting pair, and $Q(k, K)$ is the angle-averaged Pauli operator. The excitation energy of a state with relative momentum k is $k^2+\gamma^2$ (this defines γ^2). For numerical work, (3.11) is more useful than (3.10).

In our notation, a state such as $\mid mn\rangle$ or $\mid \zeta_{mn}\rangle$ contains a plane wave in the center-of-mass coordinate $\mathbf{R}$ as well as a normalization factor Ω^{-1}, e.g.,

$$\mid mn\rangle = \Omega^{-1} \exp(i\mathbf{K}\cdot\mathbf{R}) \mid \mathbf{k}_0Sm_S\rangle. \quad (3.12)$$

Thus the matrix element $\langle \zeta_{kl} \mid \zeta_{mn} - \zeta_{nm}\rangle$, which will arise later on, is given by

$$\langle \zeta_{kl} \mid \zeta_{mn} - \zeta_{nm}\rangle = \Omega^{-1} \sum_{JLL'} i^{L-L'}[1-(-1)^{L+S+T}] \times [4\pi(2L+1)]^{1/2} (L'Sm_S - m_S'm_S' \mid Jm_S) \times (LS0m_S \mid Jm_S)\, Y_{L'm_S-m_S'}(\hat{k}, \hat{k}_0) \times 4\pi \sum_{L''} \int_0^\infty \chi_{L'L''}{}^{JS}(k, r) \chi_{LL''}{}^{JS}(k_0, r)\, dr, \quad (3.13)$$

where $\mid mn\rangle$ is given by (3.12), and the corresponding quantum numbers for $\mid kl\rangle$ are $\mathbf{K}$, $\mathbf{k}$, S, m_S', with m_S and m_S' defined relative to $\mathbf{k}_0$. Each two-particle state is assumed to have a definite isospin T. The effect of the exchange term on the left-hand side of (3.13) is to give the factor $[1-(-1)^{L+S+T}]$, which selects the states that are permitted by the Pauli principle.

The expansion parameter κ is defined to be the average over occupied states m, n of the quantity

$$\kappa_{mn} = A\langle mn \mid G(mn) \frac{Q}{e(mn)} \frac{Q}{e(mn)} G(mn) \mid mn - nm\rangle = A\langle \zeta_{mn} \mid \zeta_{mn} - \zeta_{nm}\rangle. \quad (3.14)$$

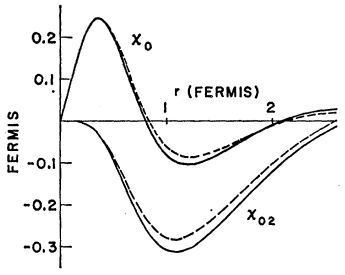

FIG. 36. Two-body defect functions for the Reid soft-core potential. The curves labeled χ_0 are for the $^1S_0$ entrance channel. The curves labeled χ_{02} represent the D-wave component in the $^3S_1$ entrance channel. The solid and dashed curves are for relative momenta of 0.2 and 1.2 F^{-1}, respectively.

The average over spin and isospin is seen from (3.13) to be

$$\langle \kappa_{mn}\rangle_{S,T \text{ av.}} = \rho \sum_{JLS} \nu(LSJ) \sum_{L'} 4\pi \int_0^\infty [\chi_{LL'}{}^{JS}(k_0, r)]^2 dr, \quad (3.15)$$

$$\nu(LSJ) = \tfrac{1}{16} \sum_{T=0,1} [1-(-1)^{L+S+T}](2J+1)(2T+1), \quad (3.16)$$

where $\rho = A/\Omega$ is the particle density. Using the single-particle spectrum (3.1) at $k_F = 1.36$ F^{-1}, formula (3.15) has been averaged over momenta to obtain[6] $\kappa = 0.135$ and $\kappa = 0.193$ for the Reid[18] soft-core and hard-core potentials, respectively.

An important fact[6] that we will use later is that 90% of expression (3.15) comes from the S-wave entrance channels. Thus it is often a good approximation in formulas containing $\chi_{LL'}{}^{JS}$ to retain only terms with $L=0$. The D-wave component $\chi_{02}{}^{11}$ in the $^3S_1$ entrance channel is very important. We have found that this component alone contributes to κ about 50% of the total.

A second very useful fact is that the S-wave entrance-channel functions $\chi_{0L'}{}^{JS}$ in (3.15) depend very little on the initial momenta of the two states m, n. This is shown in Fig. 36. The $^1S_0$ defect function $\chi_{00}{}^{00} \equiv \chi_0$, and the induced D wave $\chi_{02}{}^{11} \equiv \chi_{02}$ in the $^3S_1$ entrance channel, are both plotted against r for two quite different relative momenta, $k_0 = 0.2$ F^{-1} (solid curves) and $k_0 = 1.2$ F^{-1} (dashed curves). In each case K was put equal to its rms value consistent with the given value of k_0. The function $\chi_{00}{}^{11} \equiv \chi_{00}$ is not shown but is very similar to χ_0.

In view of the above discussion, it is clear that κ_{mn} is nearly independent of the momenta of m, n. Figure 37 shows a plot of the spin-isospin average of κ_{mn} against the relative momentum k_0. It is clear that deviations of κ_{mn} from its average value by more than 5% are highly improbable. We will make repeated use of the fact that κ_{mn} is nearly constant.

A number of four-hole-line diagrams contain optional

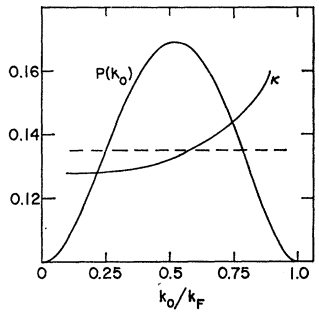

FIG. 37. Curve labeled κ shows the dependence of κ_{mn} on the relative momentum k_0 of states m and n. The left-hand vertical scale is used. The horizontal dashed line represents the average of κ_{mn} over m, n. The curve labeled $P(k_0)$ gives the probability of finding two occupied states m, n with relative momentum k_0. This curve is in arbitrary units and goes to zero at $k_0=0$ and $k_0=k_F$.

particle-particle interactions. Suppose that W_1 is the contribution obtained without the optional particle-particle interaction, and that W_2 is the contribution obtained when this interaction is included. Then W_2 contains a factor G/e relative to W_1. This G matrix is taken between highly excited states and is usually positive. The additional energy denominator gives a minus sign. Hence W_2 cancels part of W_1. This motivates us to introduce a reduction factor r defined by

$$W_1+W_2=rW_1. \tag{3.17}$$

Let us estimate this reduction factor for class A5. Omitting a common factor, we find from (2.14)

$$W_1=\sum_{ab}\langle\zeta_{lm}\mid ab\rangle(E_a+E_b+E_c-E_k-E_l-E_n)^{-1}\times\langle ab\mid\zeta_{lm}-\zeta_{ml}\rangle, \tag{3.18}$$

$$W_2=-\sum_{abde}\langle\zeta_{lm}\mid ab\rangle(E_a+E_b+E_c-E_k-E_l-E_n)^{-1}\times\langle ab\mid G(lkn;c)[Q/e(lkn;c)]\mid de\rangle\langle de\mid\zeta_{lm}-\zeta_{ml}\rangle. \tag{3.19}$$

Let $\mid lm\rangle$ have relative momentum $\mathbf{k}_0$ and spin-isospin quantum numbers $Sm_ST\tau_3$, while the corresponding quantities for $\mid ab\rangle$ are $\mathbf{k}$ $Sm_S'T\tau_3$. Then the matrix elements in (3.18) can be obtained from (3.9) [including an exchange term as in (3.13)], and the sum over ab becomes an integral over $\mathbf{k}$. Expression (3.18) depends on the direction of $\mathbf{k}$ through the spherical harmonics that come from (3.9) and through the requirement that $\mathbf{a}=\frac{1}{2}\mathbf{K}_{ab}+\mathbf{k}$ and $\mathbf{b}=\frac{1}{2}\mathbf{K}_{ab}-\mathbf{k}$ both lie above the Fermi sea, where $\mathbf{K}_{ab}=\mathbf{K}_{lm}\equiv\mathbf{K}$. Our treatment of this last requirement is analogous to our use of the angle-averaged Pauli operator: We average over directions of $\mathbf{k}$ and insert a factor $Q(k, K)$. This allows us to benefit from the orthogonality of the spherical harmonics, which in turn greatly simplifies the sum over spin and isospin. After summing over all spin and isospin quantum numbers, we obtain

$$\sum_{Sm_S,TT_3}W_1=16\sum_{SJLL'}\nu(LSJ)\int\frac{d^3k}{(2\pi)^3}[\chi_{LL'}{}^{JS}(k,k_0)]^2\times\frac{Q(k,K)}{k^2+\gamma_3{}^2}, \tag{3.20}$$

$$\gamma_3{}^2=\tfrac{1}{4}K_{ab}{}^2+E_c-E_k-E_l-E_n. \tag{3.21}$$

In (3.19) the sum over de can be evaluated by closure to give $\langle\zeta_{ab}\mid\zeta_{lm}-\zeta_{ml}\rangle$, where ζ_{ab} must be calculated with the starting energy $(E_k+E_l+E_n-E_c)$. Proceeding in the same way as for (3.18), and using (3.13), now gives

$$\sum_{Sm_S,TT_3}W_2=-16\sum_{SJLL'}\nu(LSJ)\int\frac{d^3k}{(2\pi)^3}\times\chi_{LL'}{}^{JS}(k,k_0)B_{LL'}{}^{JS}(k,k_0)\frac{Q(k,K)}{k^2+\gamma_3{}^2}, \tag{3.22}$$

$$B_{LL'}{}^{JS}(k,k_0)=4\pi\sum_{L''}\int_0^\infty\chi_{L'L''}{}^{JS}(k,r)\chi_{LL''}{}^{JS}(k_0,r)\,dr. \tag{3.23}$$

Note that we would have $W_1+W_2=0$, i.e., a perfect cancellation, if $\chi_{L'L''}{}^{JS}(k, r)$ were replaced in (3.23) by $\delta(L', L'')rj_{L'}(kr)$. This replacement is exact inside the core radius (if any), but it is wrong for larger r.

In accord with our earlier discussion, we included only terms with $L=0$ in the numerical evaluation of (3.20) and (3.22), and we calculated only for one value of k_0, namely, $k_0=\frac{1}{2}k_F=0.68$ F^{-1}. To obtain a reasonable value for $\gamma_3{}^2$, note first that $\mathbf{K}_{ab}=\mathbf{K}_{lm}$ so that

$$\tfrac{1}{4}K_{ab}{}^2=\tfrac{1}{4}(\mathbf{l}+\mathbf{m})^2=\tfrac{1}{4}(l^2+m^2+\mathbf{l}\cdot\mathbf{m}).$$

On the average, $\mathbf{l}\cdot\mathbf{m}$ is zero, and the average value of l^2 is $0.6k_F{}^2$. So we replace $\frac{1}{4}K_{ab}{}^2$ by $0.3k_F{}^2$. The momentum of c is restricted by momentum conservation to be between k_F and $3k_F$. Taking $c=1.5k_F$ gives $E_c=1.125k_F{}^2$. Finally, we put $(E_k+E_l+E_n)=3\bar{E}$, where $\bar{E}=-43$ MeV is the average single-particle energy for the spectrum (3.1). Thus we get

$$\gamma_3{}^2=1.425k_F{}^2-3\bar{E}=5.75\text{ F}^{-2}. \tag{3.24}$$

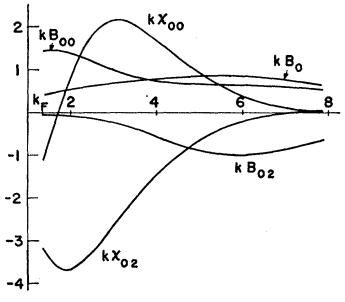

FIG. 38. Various functions of relative momentum k that arise in the calculation of the reduction factor for class A5 and are defined in the text. The horizontal axis represents k in units of F^{-1}. The dimensions of the vertical axis are F^2. The function $k\chi_0(k, k_0)$ is not shown but is very similar to $k\chi_{00}$.

There is no need to treat γ_3^2 more carefully. Note that this off-energy-shell value of γ_3^2 is also used in calculating the function $\chi_{L'L''}{}^{JS}(k, r)$ that appears in (3.23). The defect functions with initial relative momentum k_0 were calculated using the on-energy-shell value of γ^2 appropriate to the spectrum (3.1), given by

$$\gamma^2=2A_1-k_0^2/m^*+\tfrac{1}{4}K^2(1-1/m^*). \quad (3.25)$$

In order to simplify the function $Q(k, K)$ in (3.20) and (3.22), we took $K=0$. For the on-energy-shell wave functions we then find $\gamma^2=3.14$ F^{-2} from (3.25).

The χ's and B's, multiplied by k, are plotted against k in Fig. 38. The product $\chi_{02}B_{02}$ is much smaller than $(\chi_{02})^2$ for most values of k. This means that the D wave induced by the tensor force produces very little cancellation between (3.20) and (3.22). But the cancellation in the $^1S_0$ state is appreciable, as is that in the S wave of the $^3S_1$ entrance channel.

The reduction factor calculated from B_{02} and χ_{02} alone is 0.94; from B_{00} and χ_{00} alone it is 0.48; from B_0 and χ_0 alone it is 0.53. The complete reduction factor r comes to 0.80. Thus the optional particle-particle interaction in class A5 produces a 20% cancellation. Another interesting quantity is the average value of $k^2+\gamma_3^2$, defined as the ratio of (3.20) [calculated *without* the factor $(k^2+\gamma_3^2)^{-1}$] to (3.20) as given. The result is 530 MeV.

We have now set down enough formulas to permit an accurate evaluation of the two-body combination diagrams. Our treatment of diagrams that require a detailed knowledge of the three-body functions Z_1 and Y will be much less accurate. We will completely ignore the tensor force and use the approximation of Ref. 12, which gives Z_1 as a polynomial of two-body correlation functions. This result was derived for a potential with a hard core, but we will use it for our qualitatively similar potential with a Yukawa core. Also, we use only the S-wave components of the two-body correlation functions that appear in the formula for Z_1. Our results will be of the correct order of magnitude for central forces, but we cannot claim high accuracy. And additional uncertainty is introduced by our omission of the tensor force. Similar approximations will be made in the evaluation of the four-body clusters.

We will need in the numerical work the contributions W_3 and $W_3^{\rm hh}$ from the three-body cluster diagrams and the hole-hole diagram, respectively. For W_3 we take the results of Dahlblom (using the Reid *hard-core* potential)

TABLE I. Values of various parameters defined in the text.

k_F	1.36 F^{-1}
$\bar{U}$	−66 MeV
$\bar{E}$	−43 MeV
κ	0.135
r	0.8
W_3	−1.1 MeV
$W_3^{\rm hh}$	−0.34 MeV

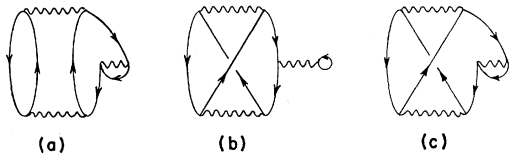

FIG. 39. Exchange diagrams corresponding to the direct diagram of Fig. 1(d).

that are quoted by Rajaraman and Bethe.[14] The sum of various terms in W_3 quoted near the end of Sec. 6 of their paper is −1.1 MeV. We calculate $W_3^{\rm hh}$ in the present paper to be −0.34 MeV. We conclude our preliminary remarks by listing in Table I the values of various parameters used in the numerical work.

B. Hole-Hole Diagram

We now calculate the contribution from the hole-hole diagram of Fig. 1(e). This diagram has only three independent hole lines. But it has not been carefully calculated before, and we need to know its size in order to estimate some of the four-hole-line diagrams.

The contribution to the energy per particle of the hole-hole diagram is

$$W_3^{\rm hh}=A^{-1}\tfrac{1}{2}\sum\langle\zeta_{jn}\,|\,\zeta_{lm}-\zeta_{mt}\rangle\langle lm\,|\,G(jn)\,|\,jn\rangle. \quad (3.26)$$

We first make a rough but simple estimate of this expression. This will serve to introduce ideas that will later be used in making rough estimates of four-hole-line diagrams.

The first requirement for our rough estimate is an approximate way of including all exchange diagrams. We assume a spin-independent central potential. Since a typical intermediate-state momentum is much larger than a typical momentum in the Fermi sea, we may approximate all hole momenta by zero. With these simplifications, it may happen that the contributions from the various exchange diagrams differ only in sign and in the statistical weight due to spin-isospin summations. This is the case when the exchange diagrams are obtained by permutation of hole lines at the top or bottom of the diagram,[3,13,14] as in the three-body combination and four-body cluster diagrams. It is also true for two-body-combination diagrams whenever all exchange diagrams can be obtained by exchanging *hole* lines in various two-body interactions. For example, under exchange the spatial part of the matrix element $\langle 00\,|\,G\,|\,\mathbf{k}-\mathbf{k}\rangle$ is unchanged, and the only possible change is in the spin-isospin part. We assume that one of these favorable situations occurs. Then diagrams that differ by an odd number of closed loops will differ in sign. And the number of independent spin-isospin summations is equal to the number of closed loops because, for a spin-independent central potential, every line in a given closed loop must have the same spin and isospin. Since there are four spin-isospin states for a nucleon, reducing the number of closed loops in any diagram by one multiplies its contribution

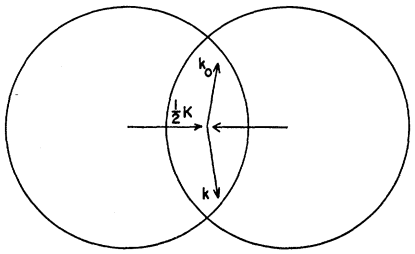

FIG. 40. Two intersecting Fermi spheres that are used in the calculation of phase-space factors. Each sphere has radius k_F, and their centers are separated by a distance K.

by $-\frac{1}{4}$. Arbitrarily choosing one diagram as the direct diagram, we can write the total contribution from all the diagrams as a statistical weight times the contribution from the direct diagram alone. This statistical weight is the sum of the statistical weights of each of the individual diagrams. By definition, the statistical weight of the direct diagram is unity. Diagrams with one less closed loop have a weight of $-\frac{1}{4}$, those with two fewer loops have a weight of $\frac{1}{16}$, etc.

These ideas have been stated and used by Rajaraman.[36] As a simple example, take the direct diagram to be that of Fig. 1(d), and let the exchange diagrams be those of Figs. 39(a)-39(c). The statistical weights of the four diagrams are 1, $-\frac{1}{4}$, $-\frac{1}{4}$, $+\frac{1}{16}$, respectively. Thus the sum of all four diagrams is approximately $\frac{9}{16}$ times the direct diagram.

Having discussed the inclusion of exchange in our rough estimates, we consider next the approximate summation over states in the Fermi sea. After momentum conservation has been taken into account, each four-hole-line diagram involves four summations over occupied states. In the approximation of zero hole momentum, all dependence on hole momenta is neglected, and each summation over momenta in the Fermi sea simply gives a factor $\frac{1}{4}A$. Each independent spin-isospin summation gives a factor of 4, but it must be remembered that the number of independent spin-isospins is equal to the number of closed loops. For example, the summation over occupied states for a four-hole-line diagram with only two closed loops gives a factor $\frac{1}{16}A^4$.

A complication that often arises in summing over occupied states can be illustrated by means of the hole-hole diagram. In expression (3.26) we can allow $\mathbf{j}$ to be determined by momentum conservation and sum over $\mathbf{l}$, $\mathbf{m}$, and $\mathbf{n}$ in the Fermi sea, subject to the restriction $|\mathbf{j}|=|\mathbf{l}+\mathbf{m}-\mathbf{n}|<k_F$. This amounts to summing independently over $\mathbf{l}$, $\mathbf{m}$, $\mathbf{n}$ and then multiplying by the phase-space factor

$$f=(\tfrac{4}{3}\pi k_F^3)^{-3}\int d\mathbf{l}d\mathbf{m}d\mathbf{n}, \qquad |\mathbf{l}+\mathbf{m}-\mathbf{n}|<k_F. \quad (3.27)$$

To compute f, we introduce the relative and center-of-mass variables

$$\mathbf{K}=\mathbf{l}+\mathbf{m}, \qquad \mathbf{k}_0=\tfrac{1}{2}(\mathbf{l}-\mathbf{m}), \qquad \mathbf{k}=\tfrac{1}{2}(\mathbf{j}-\mathbf{n}). \quad (3.28)$$

[36] R. Rajaraman, Phys. Rev. 129, 265 (1963).

For a given $\mathbf{K}$, the tips of the vectors $\mathbf{k}$ and $\mathbf{k}_0$ can vary independently over the intersection of the two spheres shown in Fig. 40. Each sphere has radius k_F, and their centers are a distance K apart. Using these new variables, it is easy to obtain the result $f=34/105$, which for all practical purposes becomes $f=\frac{1}{3}$.

In making rough estimates, we will often replace matrix elements by their average values. Consider the matrix element $\langle\zeta_{jn}\,|\,\zeta_{lm}\rangle$, which is approximated by $\Omega^{-1}\int\zeta^2 d\tau$ when the slight dependence of ζ on the initial momenta is neglected. This last integral is related to κ. Since we assume a spin-independent central potential, and since only S waves are important for κ, exchange gives a factor $\frac{3}{4}$ and we get

$$\kappa\approx\tfrac{3}{4}\rho\int\zeta^2 d\tau. \quad (3.29)$$

It is now clear that

$$\langle\zeta_{jn}\,|\,\zeta_{lm}\rangle\approx 4\kappa/3A \quad (3.30)$$

and we will often use this approximation.

The same ideas can be applied to matrix elements of G between low-lying states. The contributions from odd states tend to cancel out in such matrix elements, and exchange simply gives a factor $\frac{3}{4}$ for even states. Thus we have

$$U(m)=\sum_n\langle mn\,|\,G\,|\,mn-nm\rangle\approx\tfrac{3}{4}\sum_n\Omega^{-1}\bar{G}, \quad (3.31)$$

$$\bar{U}\approx\tfrac{3}{4}\rho\bar{G}. \quad (3.32)$$

This leads to the approximation

$$\langle lm\,|\,G\,|\,jn\rangle\approx\Omega^{-1}\bar{G}\approx 4\bar{U}/3A \quad (3.33)$$

for an average matrix element of G between states of low momentum.

We now have the ingredients necessary for rough estimates of four-hole-line diagrams. We will illustrate their use by making a rough estimate of the hole-hole diagram. There is only one exchange diagram in addition to the direct diagram of Fig. 1(e), and the total statistical weight is $1-\frac{1}{4}=\frac{3}{4}$. The direct diagram has three independent summations over occupied states but only two closed loops; hence these summations give a factor $\frac{1}{4}A^3$. The restriction $|\mathbf{l}+\mathbf{m}-\mathbf{n}|<k_F$ introduces the phase-space factor $\frac{1}{3}$. The matrix elements $\langle\zeta_{jn}\,|\,\zeta_{lm}\rangle$ and $\langle lm\,|\,G\,|\,jn\rangle$ that occur in the direct diagram are replaced by formulas (3.30) and (3.33), respectively. Combining all these factors with the factor $\frac{1}{2}A^{-1}$ that already appears in (3.26), we obtain

$$W_3^{\rm hh}\approx\frac{1}{2}A^{-1}\frac{3}{4}\frac{A^3}{4}\frac{1}{3}\frac{4\kappa}{3A}\frac{4\bar{U}}{3A},$$

$$W_3^{\rm hh}\approx\kappa\bar{U}/18=-0.48\ \text{MeV}. \quad (3.34)$$

The effect of the tensor force will be largely included in this formula by using the correct values of κ and $\bar{U}$, calculated with the tensor force included.

Approximate formulas such as (3.34) are extremely useful. They give an idea of the numerical importance of a diagram without tedious calculation. Further-

more, although the numerical factor 1/18 is only a rough approximation, the result that $W_3^{\rm hh}$ scales as $\kappa\bar{U}$ should be reliable. Hence an accurate calculation of $W_3^{\rm hh}$ with a given two-body potential at a given density can be extrapolated to other two-body potentials and to other densities. To make the extrapolation one has only to know the values of κ and $\bar{U}$ for the new potential or density.

Having described the methods to be used in making rough estimates, we turn to an accurate calculation of $W_3^{\rm hh}$. Each of the two matrix elements in (3.26) is written as a sum of partial-wave contributions by using (3.7) and (3.13). All the dependence on the directions of the relative momenta $\mathbf{k}$, $\mathbf{k}_0$ [defined by (3.28)] is now contained in a factor of the form

$$Y_{l'm'}{}^*(\hat{k},\hat{k}_0)\,Y_{lm}(\hat{k},\hat{k}_0).$$

We average over the angle between $\mathbf{k}$ and $\mathbf{k}_0$ to get $\delta(l,l')\delta(m,m')$. Then the orthogonality relations for Clebsch-Gordan coefficients can be used to greatly simplify the formula. The final result is

$$W_3^{\rm hh}=\tfrac{1}{2}\rho^{-1}(2\pi)^{-9}\int d\mathbf{K}\,d\mathbf{k}\,d\mathbf{k}_0\sum_{LSJ}16\nu(LSJ)\times\sum_{L'}G_{LL'}{}^{JS}(k,k_0)\sum_{L''}4\pi\times\int\chi_{L'L''}{}^{JS}(k,r)\chi_{LL''}{}^{JS}(k_0,r)\,dr. \quad (3.35)$$

Averaging over the angle between $\mathbf{k}$ and $\mathbf{k}_0$ is only an approximation, as can be seen from Fig. 40. The trouble is that the vector $\mathbf{k}$, for example, is not free to point in any direction unless its magnitude is less than $k_F-\frac{1}{2}K$. However, if either $|\mathbf{k}|$ or $|\mathbf{k}_0|$ is less than $k_F-\frac{1}{2}K$, the angle averaging is justified. The angle averaging is exact in 74% of the available phase space and is probably quite a good approximation in the remainder. So we do not expect any serious error from this source.

Let us now consider what values of L, L', L'' are important in (3.35). Terms with $L=L'=0$ and $L''=0$, 2 are clearly important. Terms with $L=0$, $L'=2$ are negligible because the defect function χ is so small in the ${}^3D_1$ entrance channel. This was checked by calculating the sum over L'' of the spatial integral appearing in (3.35). We took $k=k_F$ in order to make $\chi_{2L''}(k,r)$ as large as possible. For all values of k_0, the result was about 1% of that obtained with $L=L'=0$. Thus terms with $L=0$, $L'=2$ are negligible, and so, therefore, are terms with $L=L'=2$.

The only possibility remaining is $L=L'=1$. The P-wave defect function is not negligible, the P-wave contribution to κ being 10% of the S-wave contribution. But the P-wave matrix elements $G_{11}{}^{JS}$ are sometimes positive and sometimes negative (depending on J, S) and tend to cancel out. The extent of this cancellation was tested as follows: First, we replaced $\nu(1SJ)G_{11}{}^{JS}(k,k_0)$ by the contribution of that particular P-wave entrance channel to the first-order binding energy (Table 6 of Ref. 6). The sum over L'' of the integral of $(\chi_{1L''}{}^{JS})^2$ was then estimated by using the contribution to κ from that particular entrance channel (Table 6, Ref. 6). These two numbers were multiplied together for the ${}^1P_1$, ${}^3P_0$, ${}^3P_1$, and ${}^3P_2$ entrance channels, and the results were summed. The final result was 200 times smaller than the corresponding result for $L=L'=0$. We conclude that it is an excellent approximation to include only terms with $L=L'=0$ in (3.35).

Since the defect functions in the S-wave entrance channel are nearly independent of the initial relative momentum, the integral of the product of two χ's in (3.35) was replaced by a constant, independent of k and k_0. Allowing k and k_0 to range independently from $0.1\,k_F$ to $0.9\,k_F$, we found that the value of this integral remained constant to within 16%. For k and k_0 between $0.3\,k_F$ and $0.7\,k_F$, the variation was 8%. We actually used the average over k_0 of the value obtained with $k=k_0$ (Multiplying this value by $\frac{3}{8}\rho$ gives the contribution to κ from the ${}^1S_0$ and ${}^3S_1$ entrance channels).

Having made the above approximations, we calculated the integral over allowed values of $\mathbf{K}$, $\mathbf{k}$, and $\mathbf{k}_0$ numerically. The required values of $G_{00}(k,k_0)$ were obtained by interpolation from an array of previously calculated values. The result for $W_3^{\rm hh}$ was -0.34 MeV. The error due to our approximations is probably about 10%.

We can use this result for the soft-core potential along with (3.34) to estimate $W_3^{\rm hh}$ for the Reid[18] hard-core potential at normal density. Both potentials have about the same value of $\bar{U}$, but the value of κ is 43% larger for the hard-core potential.[6] Thus $W_3^{\rm hh}$ is about 43% larger for the hard-core potential, i.e., $W_3^{\rm hh}\approx -0.49$ MeV for the hard-core potential at $k_F=1.36$ F^{-1}.

C. Two-Body Combination Diagrams

Class A1. Using closure to carry out the summations over a, b, c, and d in Eq. (2.4), we obtain

$$W(\mathrm{A1})=A^{-1}\tfrac{1}{2}\sum\langle\zeta_{lm}\,|\,\zeta_{lm}-\zeta_{ml}\rangle\langle\zeta_{nk}\,|\,\zeta_{nk}-\zeta_{kn}\rangle\times\langle mn\,|\,G\,|\,mn-nm\rangle. \quad (3.36)$$

Now, from (3.14), we see that

$$\sum_l\langle\zeta_{lm}\,|\,\zeta_{lm}-\zeta_{ml}\rangle=A^{-1}\sum_l\kappa_{lm}\cong\kappa. \quad (3.37)$$

This is an excellent approximation because κ_{lm} already depends very little on $\mathbf{m}$ and averaging over $\mathbf{l}$ reduces this dependence on $\mathbf{m}$ even further [the left-hand expression in (3.37) is clearly independent of the spin and isospin of m]. The sum over k in (3.36) is carried out in analogy with (3.37), and we obtain

$$W(\mathrm{A1})\cong A^{-1}\tfrac{1}{2}\sum_{mn}\kappa^2\langle mn\,|\,G\,|\,mn-nm\rangle=\tfrac{1}{2}\kappa^2\bar{U}. \quad (3.38)$$

Using the values of κ and $\bar{U}$ from Table I gives $W(\mathrm{A1})=-0.60$ MeV. This very simple estimate should be accurate to within a few percent, and a more elaborate calculation is unnecessary. Note that the tensor force is fully taken into account.

The expression $\frac{1}{2}\kappa^2 U$ is exactly equal to κ^2 times the two-hole-line contribution to the binding energy. This is the order of magnitude that was expected *a priori* for a typical four-hole-line diagram. Recalling our discussion of rough estimates in Sec. III B, we can now see that most four-hole-line contributions will in fact be much smaller than this. For example, the diagram of class A1 has four closed loops. If it had only three closed loops, as is the case for many four-hole-line diagrams, its contribution would be reduced by a factor of 4. Also, class A1 involves no phase-space factors such as the one that reduces the contribution of the hole-hole diagram by a factor of 3. The contribution of class A1 also tends to be large because of a "coherence effect:" in summing formula (2.4) over the momentum indices, we find that every term has the same sign. There is no cancellation between contributions from different regions of momentum space. For the vast majority of four-hole-line diagrams, circumstances are not so favorable as they are for class A1, and most four-hole-line contributions are accordingly much smaller than $W(\mathrm{A1})$.

The contribution from class A1 has been previously calculated by Brueckner, Gammel, and Kubis,[25] using the BGT[10] potential. Their result of -1.5 MeV for the sum of classes A1 and A5 is about twice as large as ours. The discrepancy suggests that the value of κ appropriate to the Brueckner-Gammel-Kubis calculation is about 50% larger than the value used in the present work. This is perfectly reasonable since their potential had a hard core, and they worked at a higher particle density. Köhler[26] used formula (3.38) to obtain a result of -2.1 MeV for the Hamada-Johnston[19] potential. This is consistent with his calculated value of κ which was 0.25.

Class A2. The first two matrix elements in (2.7) can be summed over a, b, and l by using (3.37). The remaining factors in (2.7) are the same as those in the hole-hole diagram, except for a factor of 2. When the approximation (3.37) is made, the contribution from Fig. 6(b) becomes equal to that from Fig. 6(a). Inserting an additional factor of 2 to account for Fig. 6(b), we find

$$W(\mathrm{A2})\cong -4\kappa W_3^{\mathrm{hh}}=0.18\ \mathrm{MeV}. \tag{3.39}$$

This estimate includes the tensor force and should be accurate to a few percent for a given value of W_3^{hh}.

Class A3. To evaluate class A3, we plan to calculate $U(b)$ from (2.10) and put the result into (2.9). Let $|nk\rangle$ have relative momentum $\mathbf{k}_0$ and spin-isospin quantum numbers Sm_STT_3, and let the corresponding quantities for $|bc\rangle$ be $\mathbf{k}'Sm_S'TT_3$ (m_S and m_S' are both referred to the polar axis $\mathbf{k}_0$). Partial-wave expansions for the matrix elements that appear in (2.10) are obtained from (3.7) and (3.9). The product of these two partial-wave expansions contains the product of two spherical harmonics, both with argument $(\hat{k}', \hat{k}_0)$. We make the approximation of averaging over the angle between $\mathbf{k}'$ and $\mathbf{k}_0$. The orthogonality of the spherical harmonics then greatly simplifies the formulas.

The next step is to sum over all spin and isospin quantum numbers. This implies a summation over the spin and isospin of b, which should be kept fixed when evaluating (2.10). A factor of $\frac{1}{4}$ is inserted to correct for this overcounting. This procedure is permissible because $U(b)$ is independent of the spin and isospin of b. The result is (including the overcounting factor of $\frac{1}{4}$)

$$\tfrac{1}{4}\sum_{Sm_Sm_S',TT_3}\langle nk\,|\,G\,|\,bc\rangle\langle bc\,|\,(Q/e)G\,|\,nk-kn\rangle \cong\tfrac{1}{4}\Omega^{-2}\sum_{JLS}16v(LSJ)\sum_{L'}G_{LL'}{}^{JS}(k',k_0)\chi_{LL'}{}^{JS}(k',k_0). \tag{3.40}$$

The sum over momenta $\mathbf{k}$, $\mathbf{n}$, and $\mathbf{c}$ gives a factor $(\frac{1}{4}A)^2$ times an average over $\mathbf{k}_0$, $\mathbf{K}$, with $\mathbf{c}=\mathbf{K}-\mathbf{b}$ being determined from momentum conservation ($\mathbf{K}$ is the total momentum of the state $|nk\rangle$). A numerical integration over k_0 was carried out, each point being weighted by the probability

$$P(k_0)\,dk_0=24x^2(1-\tfrac{3}{2}x+\tfrac{1}{2}x^3)\,dx \tag{3.41}$$

for finding two particles in the Fermi sea with relative momentum between k_0 and k_0+dk_0 [In(3.41), $x=k_0/k_F$].

In contrast to the integral over k_0, the integral over $\mathbf{K}$ was not evaluated in detail. Instead, for a given value of k_0, K was put equal to its rms value, determined from

$$\langle K^2\rangle_{\mathrm{av}}=2.4k_F^2(1-x)\,(x^2+3x+6)/(6+3x), \tag{3.42}$$

where $x=k_0/k_F$. This value of K was used in two ways. First, for given values of K and b, the relations $\mathbf{c}=\mathbf{K}-\mathbf{b}$ and $|\mathbf{c}|>k_F$ permit only certain directions of $\mathbf{K}$ relative to $\mathbf{b}$. The fraction of the total solid angle that is available to $\mathbf{K}$ is

$$\begin{aligned} f(b,K)&=[(b+K)^2-k_F^2]/4Kb, && b<k_F+K\\ &=1, && b>k_F+K. \end{aligned} \tag{3.43}$$

This phase-space factor is inserted into (3.40). The second use of K is to determine an average value of $k'=\frac{1}{2}|\mathbf{b}-\mathbf{c}|$. Using $\mathbf{k}'=\frac{1}{2}\mathbf{K}+\mathbf{b}$, we average k'^2 over the allowed directions of $\mathbf{K}$ relative to $\mathbf{b}$ to get

$$\begin{aligned} \langle k'^2\rangle_{\mathrm{av}}&=\tfrac{3}{4}b^2+\tfrac{1}{4}k_F^2+\tfrac{1}{2}Kb, && b<k_F+K\\ &=b^2+\tfrac{1}{4}K^2, && b>k_F+K. \end{aligned} \tag{3.44}$$

This value of k' was used in (3.40).

Thus the final expression used to calculate $U(b)$ is

$$U(b)=\tfrac{1}{4}\rho^2\int_0^{k_F}P(k_0)\,dk_0 f(b,K)\times\sum_{JLL'S}\nu(LSJ)G_{LL'}{}^{JS}(k',k_0)\chi_{LL'}{}^{JS}(k',k_0). \quad (3.45)$$

For each value of k_0, the values of K and k' are determined from (3.42) and (3.44), respectively. Because of the various approximations made, we cannot claim high accuracy for this formula. It is perhaps good to 30% for b just above the Fermi sea, and it should become more accurate as b increases.

The entrance channels JLS included in the evaluation of (3.45) were $^1S_0$, $^3S_1$, $^1P_1$, $^3P_0$, $^3P_1$, and $^3P_2$. The D-wave entrance channels were found to give a negligible contribution. The $^3S_1$ state accounted for more than half the total, and the P waves contributed about 15% as much as the S waves. There is no cancellation among various P-wave contributions because, since $\chi_{LL'}$ is given by (3.11), all matrix elements of G in (3.45) are *squared*. The calculated values of $U(b)$ are plotted in Fig. 41.

For a fixed value of b in (2.9), the sum over a, l, and m is carried out in analogy with our treatment of (2.10). The result is then integrated over $\mathbf{b}$. The final expression is

$$W(\mathrm{A3})=\int\frac{d^3b}{(2\pi)^3}U(b)\rho\sum_{JLL'S}\nu(LSJ)\times\int P(k_0)\,dk_0 f(b,K)[\chi_{LL'}{}^{JS}(k',k_0)]^2, \quad (3.46)$$

from which we obtain $W(\mathrm{A3})=0.26$ MeV.

Class A4. In formula (2.12) for $W(\mathrm{A4})$ we convert the summation over momenta $\mathbf{a}$, $\mathbf{b}$, $\mathbf{c}$, and $\mathbf{d}$ to an integration over coordinate space to obtain

$$W(\mathrm{A4})=-\tfrac{1}{2}A^{-1}\sum_{lmnk}\int d\tau_1\,d\tau_2\,d\tau_3\,d\tau_4\times[\zeta_{lk}(1,4)-\zeta_{kl}(1,4)]^*\{v(2,3)\times[\psi_{nm}(2,3)-\psi_{mn}(2,3)]\}^*[\zeta_{nk}(2,4)-\zeta_{kn}(2,4)]\times[\zeta_{lm}(1,3)-\zeta_{ml}(1,3)]. \quad (3.47)$$

Now, we have seen that in a matrix element such as $\langle ab\mid(Q/e)G\mid lm\rangle=\langle ab\mid\zeta_{lm}\rangle$, which occurs in (2.12), it is a good approximation to take only S-wave entrance channels in the state $\mid lm\rangle$. Therefore, in (3.47),

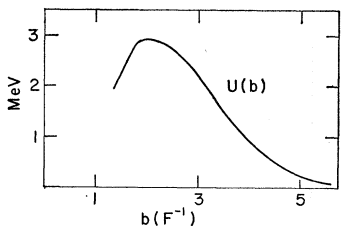

FIG. 41. On-energy-shell potential energy $U(b)$ for particle states.

we will include only S-wave entrance channels in the partial-wave expansion of each wave function. This is a great simplification because it removes all dependence on the angle between $\mathbf{k}_0$ and $\mathbf{r}$ in each two-body wave function.

Our second approximation is to neglect the dependence of the two-body wave functions on the initial relative momenta. This was shown to be accurate for the ζ's in Sec. III A. It is inaccurate for $\psi(2,3)$ only when r_{23} is large, and this does not matter because $v(2,3)$ is small in this region. So we have used the average relative momentum $(0.3)^{1/2}k_F$ in calculating each of the wave functions in (3.47). The sum over momenta $\mathbf{lmnk}$ then simply gives a factor $(\frac{1}{4}A)^4$.

To accomplish the sum over spin and isospin of l, m, n, k, we write the S-wave-entrance-channel part of ζ_{lm} in the form

$$\zeta_{lm}(1,3)-\zeta_{ml}(1,3)=\Omega^{-1}r_{13}^{-1}\times\exp[\tfrac{1}{2}i(\mathbf{l}+\mathbf{m})\cdot(\mathbf{r}_1+\mathbf{r}_3)]\times[\chi_0(r_{13})P_{13}{}^S+(\chi_{00}(r_{13})+8^{-1/2}\chi_{02}(r_{13})S_{13})P_{13}{}^T]\times(1-E_{13}{}^\sigma E_{13}{}^\tau)\mid\sigma_l\tau_l\sigma_m\tau_m\rangle. \quad (3.48)$$

The plane wave in (3.48) is the center-of-mass part of the wave function, and $\mid\sigma_l\tau_l\sigma_m\tau_m\rangle$ is a two-particle spin-isospin function. The tensor operator is denoted by S_{13}, and $P_{13}{}^S$, $P_{13}{}^T$ are singlet and triplet spin projection operators, respectively. The operators $E_{13}{}^\sigma$ and $E_{13}{}^\tau$, which exchange the spin and isospin, respectively, of particles 1 and 3, are needed to account for the exchange term on the left-hand side of (3.48). The space exchange operator is unity since we are considering only the S-wave entrance channels. The operators S_{13}, $P_{13}{}^S$, $P_{13}{}^T$, $E_{13}{}^\sigma$, and $E_{13}{}^\tau$ all have simple and well-known representations in terms of the Pauli spin operators $\boldsymbol{\sigma}_1$, $\boldsymbol{\sigma}_3$ and isospin operators $\boldsymbol{\tau}_1$, $\boldsymbol{\tau}_3$. Formulas similar to (3.48) are used for the other two-body wave functions in (3.47). The sum over spin and isospin of l, m, n, and k becomes a trace, in the spin-isospin space of four particles, of a product of four factors such as (3.48).

The evaluation of this trace requires 20 or 30 pages of algebra but is straightforward, and the result is that (3.47) becomes

$$W(\mathrm{A4})=-\tfrac{1}{2}A^{-1}\Omega^{-3}2^{-8}\times\sum_{lmnk}\int d\tau_{34}\,d\tau_1\,d\tau_2(r_{13}r_{14}r_{23}r_{24})^{-1}\times\exp[\tfrac{1}{2}i(\mathbf{l}\cdot\mathbf{r}_{34}-\mathbf{n}\cdot\mathbf{r}_{34}+\mathbf{m}\cdot\mathbf{r}_{12}-\mathbf{k}\cdot\mathbf{r}_{12})]\times V(\mathbf{r}_{14},\mathbf{r}_{23},\mathbf{r}_{24},\mathbf{r}_{13}). \quad (3.49)$$

Since the sum over spin and isospin has been carried out, only the summation over momenta remains. The plane wave comes from the center-of-mass parts of the two-body wave functions. The normalization factors Ω^{-1} carried by each of the four two-body wave functions combine to give Ω^{-4}. But after three space integrations

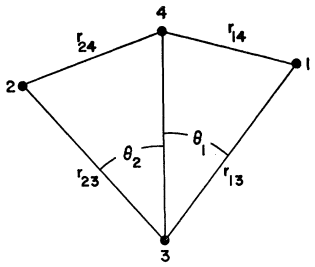

FIG. 42. Coordinate system used in the calculation of $W(\mathrm{A4})$.

have been carried out, the last one is trivial and simply gives a factor Ω. So we have changed Ω^{-4} to Ω^{-3} and written only three space integrations instead of four. The factor 2^{-8} comes from the trace calculation. The complicated function V is defined in terms of the quantities

$$\begin{aligned}
A_0(r) &= \chi_0(r)+3\chi_{00}(r),\\
A_2(r) &= -\chi_0(r)+\chi_{00}(r),\\
A_3(r) &= 2^{1/2}\chi_{02}(r),\\
G_1(r) &= v_C{}^{\mathrm{sing}}(r)\,u_0(r),\\
G_2(r) &= v_C{}^{\mathrm{trip}}(r)\,u_{00}(r)+8^{1/2}v_T(r)\,u_{02}(r),\\
C_0(r) &= G_1(r)+3G_2(r),\\
C_2(r) &= -G_1(r)+G_2(r),\\
C_3(r) &= 2^{1/2}(v_C{}^{\mathrm{trip}}-3v_{LS}-2v_T)\,u_{02}(r)+4v_T(r)\,u_{00}(r).
\end{aligned} \tag{3.50}$$

Here, a single subscript zero refers to the $^1S_0$ state, and the subscripts 00, 02 refer to the S- and D-wave components of the $^3S_1$ entrance channel. The formula for V is

$$\begin{aligned}
V(\mathbf{r}_{14},\mathbf{r}_{23},\mathbf{r}_{24},\mathbf{r}_{13}) &= 96A_0(r_{14})C_0(r_{23})A_0(r_{24})A_0(r_{13})-96A_2(r_{14})C_0(r_{23})A_0(r_{24})A_0(r_{13})+3\text{ similar terms}\\
&+192A_2(r_{14})C_2(r_{23})A_0(r_{24})A_0(r_{13})+5\text{ similar terms}-384A_2(r_{14})C_2(r_{23})A_2(r_{24})A_0(r_{13})\\
&+3\text{ similar terms}+2208A_2(r_{14})C_2(r_{23})A_2(r_{24})A_2(r_{13})+48A_3(r_{14})C_3(r_{23})A_0(r_{24})A_0(r_{13})\\
&\times[3\cos^2(\hat{r}_{14},\hat{r}_{23})-1]+5\text{ similar terms}-96A_3(r_{14})C_3(r_{23})A_2(r_{24})A_0(r_{13})\\
&\times[3\cos^2(\hat{r}_{14},\hat{r}_{23})-1]+11\text{ similar terms}+336A_3(r_{14})C_3(r_{23})A_2(r_{24})A_2(r_{13})\\
&\times[3\cos^2(\hat{r}_{14},\hat{r}_{23})-1]+5\text{ similar terms}+48A_3(r_{14})C_3(r_{23})A_3(r_{24})[A_0(r_{13})+A_2(r_{13})]\\
&\times[9\cos(\hat{r}_{14},\hat{r}_{23})\cos(\hat{r}_{14},\hat{r}_{24})\cos(\hat{r}_{23},\hat{r}_{24})-3\cos^2(\hat{r}_{14},\hat{r}_{23})-3\cos^2(\hat{r}_{14},\hat{r}_{24})-3\cos^2(\hat{r}_{23},\hat{r}_{24})+2]\\
&+3\text{ similar terms}+A_3(r_{14})C_3(r_{23})A_3(r_{24})A_3(r_{13})\{36[-30\cos(\hat{r}_{14},\hat{r}_{23})\cos(\hat{r}_{14},\hat{r}_{24})\cos(\hat{r}_{23},\hat{r}_{24})\\
&+3\text{ similar terms}+7\cos^2(\hat{r}_{14},\hat{r}_{23})+5\text{ similar terms}-7]+324\{\cos^2(\hat{r}_{14},\hat{r}_{23})\cos^2(\hat{r}_{24},\hat{r}_{13})\\
&+2\text{ similar terms}+14\cos(\hat{r}_{14},\hat{r}_{24})\cos(\hat{r}_{14},\hat{r}_{13})\cos(\hat{r}_{23},\hat{r}_{24})\cos(\hat{r}_{23},\hat{r}_{13})-2\cos(\hat{r}_{14},\hat{r}_{23})\cos(\hat{r}_{24},\hat{r}_{13})\\
&\times[\cos(\hat{r}_{14},\hat{r}_{24})\cos(\hat{r}_{23},\hat{r}_{13})+\cos(\hat{r}_{14},\hat{r}_{13})\cos(\hat{r}_{23},\hat{r}_{24})]\}).
\end{aligned} \tag{3.51}$$

To see what is meant by "similar terms" in this equation, consider the second term, which can be written symbolically in the form $A_2C_0A_0A_0$. The three similar terms are of the form $A_0C_2A_0A_0+A_0C_0A_2A_0+A_0C_0A_0A_2$.

The only dependence of (3.49) on momentum is in the plane-wave factor. So it is permissible to average each single-particle momentum independently over angles and thus convert the plane-wave factor to a product of four spherical Bessel functions of the type $j_0(\frac{1}{2}lr_{34})$.

Next, we keep $\mathbf{r}_{34}$ fixed and consider the integral of (3.49) with respect to $\mathbf{r}_1$ and $\mathbf{r}_2$, using spherical coordinates with $\mathbf{r}_{34}$ as polar axis and origin at particle 3 (see Fig. 42). The coordinates of particles 1 and 2 are $(r_{13},\theta_1,\varphi_1)$ and $(r_{23},\theta_2,\varphi_2)$, respectively. For fixed r_{34}, the function V depends on r_{13}, r_{23}, θ_1, θ_2, and $\varphi_1-\varphi_2$; hence we are faced with a five-dimensional integration. However, the integral of V with respect to $\varphi_1-\varphi_2$ can be done analytically. Furthermore, each term in the result is a *product* of a function of (r_{13},θ_1) with a function of (r_{23},θ_2). So the five-dimensional integration reduces to a sum of products of two-dimensional integrals, which is much simpler.

However, this result is spoiled by the plane wave in (3.49). The factor $j_0(\frac{1}{2}mr_{12})j_0(\frac{1}{2}kr_{12})$ prevents the integral over $\varphi_1-\varphi_2$ from being done analytically. To achieve the above simplification, we replace each of the j_0 factors by unity. This is accurate for small r_{12} and r_{34}, where the integrand is largest. A correction to this approximation will be made at the end of the calculation.

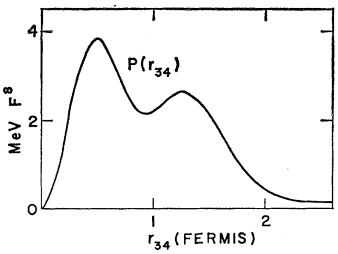

FIG. 43. Function $P(r_{34})$ that arises in the evaluation of $W(\mathrm{A4})$.

After the plane wave has been replaced by unity in (3.49), the sum over **l, m, n, k** simply gives a factor $(\frac{1}{4}A)^4$, and we get

$$W(\mathrm{A4}) = -4\pi\rho^3 \int P(r_{34})\, dr_{34}, \tag{3.52}$$

$$P(r_{34}) = 2^{-17} r_{34}^2 \int d\tau_1\, d\tau_2 (r_{13}r_{14}r_{23}r_{24})^{-1} \times V(\mathbf{r}_{14}, \mathbf{r}_{23}, \mathbf{r}_{24}, \mathbf{r}_{13}). \tag{3.53}$$

Numerical calculation gave the curve shown in Fig. 43 for $P(r_{34})$, and expression (3.52) came to -0.28 MeV.

Note that $P(r_{34})$ is negligible for $r_{34}>2$ F. Hence replacing $j_0(\frac{1}{2}lr_{34})$ by unity is a fairly good approximation. A reasonable correction to this approximation is made by computing the average of $j_0(\frac{1}{2}lr_{34})j_0(\frac{1}{2}nr_{34})$ with respect to l, n, and r_{34}, using $P(r_{34})$ as a weighting factor. The result obtained above is then multiplied by this average value. The factor $j_0(\frac{1}{2}mr_{12})j_0(\frac{1}{2}kr_{12})$ is included by multiplying once more by this *same* average value. This is because of the symmetry of the original formula (3.47) under interchange of r_{12} and r_{34}. For example, if we had chosen to integrate first over $\mathbf{r}_3$ and $\mathbf{r}_4$, keeping $\mathbf{r}_{12}$ fixed, we would again have obtained (3.52), but the variable of integration would have been r_{12} instead of r_{34}.

The average value defined above comes out to be 0.89. So our final result for $W(\mathrm{A4})$ is $-0.28(0.89)^2 = -0.22$ MeV. The importance of the tensor force is shown by repeating the calculations with $\chi_{02}(r)$ and $v_T(r)$ put equal to zero. The result is -0.06 MeV, four times smaller than the complete result including the tensor force.

Class A5. Let us first make a rough estimate of $W(\mathrm{A5})$, using the methods described in Sec. III A. The optional particle-particle interaction is included by means of the reduction factor that was calculated in Sec. III A. In addition to the direct diagram, there are three exchange diagrams, and one easily finds that the statistical weight is $1+2\times(-\frac{1}{4})+\frac{1}{16}=\frac{9}{16}$. The fact that there are four summations over occupied states and only three closed loops implies a factor $\frac{1}{4}A^4$. There is also a phase-space factor arising from the requirement that $|\mathbf{c}| = |\mathbf{k}+\mathbf{n}-\mathbf{m}| > k_F$. Let the relative momenta of states $|kn\rangle$ and $|mc\rangle$ be $\mathbf{k}_0$ and $\mathbf{k}'$, respectively, and let $\mathbf{K}$ be the total momentum of both $|kn\rangle$ and $|mc\rangle$. Then in Fig. 40 the tip of $\mathbf{k}_0$ must lie inside both spheres; and the tip of $\mathbf{k}'$ must lie inside the left-hand sphere but outside the right-hand sphere. The phase-space factor is therefore equal to one minus the phase-space factor of the hole-hole diagram, i.e., it is equal to $\frac{2}{3}$. In (2.14) the energy denominator that involves the excitation of three particles above the sea is replaced by an appropriate average value $\bar{e}$. The sum over a, b then gives a factor $\langle\zeta_{lm}|\zeta_{lm}\rangle$, which we replace by $4\kappa/3A$, as discussed in Sec. III A. Each of the remaining matrix elements of G is replaced by $4\bar{U}/3A$. Putting all these factors together, and including the reduction factor r, we obtain the rough estimate

$$W(\mathrm{A5}) \approx -A^{-1}\frac{9}{16}\frac{A^4}{4}\frac{2}{3}\frac{1}{\bar{e}}\frac{4\kappa}{3A}\left(\frac{4\bar{U}}{3A}\right)^2 r = -\frac{2}{9}\frac{r\kappa\bar{U}^2}{\bar{e}}. \tag{3.54}$$

In Sec. III A we calculated $r=0.8$ and $\bar{e}=530$ MeV. So the numerical value of (3.54) is -0.19 MeV.

To make a more accurate calculation, we note that $W(\mathrm{A5})$ is the product of expression (3.18) (summed over l) and the expression

$$-A^{-1}r \sum_{knmc} \langle kn|G|mc\rangle\langle mc|G|kn-nk\rangle. \tag{3.55}$$

It is easy to see that the sum over l of expression (3.18) is equal to $\kappa/\bar{e}$, where $\bar{e}$ was calculated to be 530 MeV in Sec. III A. To calculate (3.55), let $|kn\rangle$ and $|mc\rangle$ have quantum numbers $\mathbf{k}_0 S m_S T T_3$ and $\mathbf{k}' S m_S' T T_3$, respectively. Each matrix element in (3.55) is expanded in partial waves by using (3.7). An average over the angle between $\mathbf{k}'$ and $\mathbf{k}_0$ is made in the usual way. The spin and isospin sums are then easily carried out, and expression (3.55) becomes

$$-\rho^{-1}r(2\pi)^{-9}\int d\mathbf{K}\, d\mathbf{k}'\, d\mathbf{k}_0 \sum_{LSJL'} 16\nu(LSJ) \times [G_{LL'}{}^{JS}(k', k_0)]^2. \tag{3.56}$$

The allowed values of $\mathbf{K}$, $\mathbf{k}'$, and $\mathbf{k}_0$ have already been discussed in connection with the phase-space factor. The integration reduces to a three-dimensional integral in the variables $|\mathbf{K}|$, $|\mathbf{k}'|$, and $|\mathbf{k}_0|$ and was done numerically. All entrance channels LSJ with $J\leq 2$ were included. Averaging over the angle between $\mathbf{k}'$ and $\mathbf{k}_0$ is exact in only 35% of the available phase space. A treatment that avoids the angle averaging is feasible but has not been carried out. Using $r=0.8$, (3.56) was calculated to be -603 MeV^2. Multiplying this by $\kappa/\bar{e}$ gives $W(\mathrm{A5}) = -0.15$ MeV.

Class A6. A rough estimate of $W(\mathrm{A6})$ can be made in the same way as for class A5. We omit the optional particle-particle interaction and correct for this by using the reduction factor $r=0.8$. Replacing the middle energy denominator in Fig. 13 by its average value $\bar{e}$ leads to

$$W(\mathrm{A6}) \approx -A^{-1}(r/\bar{e}) \sum \langle\zeta_{lm}|\zeta_{kn}-\zeta_{nk}\rangle \times \langle jk|G|cl-lc\rangle\langle cn|G|jm-mj\rangle. \tag{3.57}$$

We will consider only the direct diagram, including exchange by means of a statistical weight. There are eight distinct diagrams when exchange is included, and the statistical weight is found to be $1+4\times-\frac{1}{4}+3\times\frac{1}{16}=\frac{3}{16}$.

To calculate the phase-space factor, we make the change of variables[37] (with unit Jacobian) from

[37] I am grateful to J. MacKenzie for showing me this useful transformation.

jklmnc to

$$\mathbf{K}_1=\mathbf{j}-\mathbf{c}, \quad \mathbf{K}_2=\mathbf{n}-\mathbf{m}, \quad \mathbf{K}_3=\mathbf{l}-\mathbf{k},$$
$$\mathbf{q}_1=\tfrac{1}{2}(\mathbf{j}+\mathbf{c}), \quad \mathbf{q}_2=\tfrac{1}{2}(\mathbf{n}+\mathbf{m}), \quad \mathbf{q}_3=\tfrac{1}{2}(\mathbf{l}+\mathbf{k}). \tag{3.58}$$

Momentum conservation requires that $\mathbf{K}_1=\mathbf{K}_2=\mathbf{K}_3\equiv\mathbf{K}$. Figure 40 can now be used to describe the allowed values of $\mathbf{K}$, $\mathbf{q}_1$, $\mathbf{q}_2$, and $\mathbf{q}_3$. Let the center of the two Fermi spheres be separated by a distance K, and let the vectors $\mathbf{q}_1$, $\mathbf{q}_2$, and $\mathbf{q}_3$ originate from the same point as the vectors $\mathbf{k}$, $\mathbf{k}_0$ shown in Fig. 40. Then the tip of $\mathbf{q}_1$ must lie inside the left-hand sphere but outside the right-hand sphere. The tips of $\mathbf{q}_2$ and $\mathbf{q}_3$ must both lie inside both Fermi spheres. The phase-space factor is now easily calculated to be $149/840\approx\frac{1}{6}$.

There are four summations over the Fermi sea in $W(\mathrm{A6})$, but only three closed loops. This implies a factor $\frac{1}{4}A^4$. Using the approximations (3.30) and (3.33) for the direct matrix elements in (3.57), we get

$$W(\mathrm{A6})\approx-A^{-1}\frac{r}{\bar{e}}\frac{3}{16}\frac{1}{6}\frac{A^4}{4}\frac{4\kappa}{3A}\left(\frac{4\bar{U}}{3A}\right)^2=-\frac{r\kappa\bar{U}^2}{54\bar{e}}. \tag{3.59}$$

This is 12 times smaller than our rough estimate (3.54) for $W(\mathrm{A5})$. The statistical weight due to exchange is three times smaller for class A6, and the phase-space factor is four times smaller. The numerical value of (3.59) is $W(\mathrm{A6})\approx-0.02$ MeV. A detailed computer calculation, similar to that for class A5, gave the same result.

Class A7. A rough estimate will suffice for $W(\mathrm{A7})$, which can be written

$$W(\mathrm{A7})=-\tfrac{1}{2}A^{-1}\sum\langle\zeta_{kn}\mid\zeta_{lm}-\zeta_{ml}\rangle \times\langle\zeta_{lj}\mid\zeta_{ki}-\zeta_{ik}\rangle\langle im\mid G\mid jn-nj\rangle. \tag{3.60}$$

The statistical weight due to exchange is found to be $\frac{3}{16}$. The phase-space factor is determined by introducing the new coordinates[37]

$$\mathbf{K}_1=\mathbf{m}-\mathbf{n}, \quad \mathbf{K}_2=\mathbf{k}-\mathbf{l}, \quad \mathbf{K}_3=\mathbf{j}-\mathbf{i},$$
$$\mathbf{q}_1=\tfrac{1}{2}(\mathbf{m}+\mathbf{n}), \quad \mathbf{q}_2=\tfrac{1}{2}(\mathbf{k}+\mathbf{l}), \quad \mathbf{q}_3=\tfrac{1}{2}(\mathbf{j}+\mathbf{i}). \tag{3.61}$$

Momentum conservation implies equality of the $\mathbf{K}_i$. The discussion is now the same as for class A6, except that the tip of each of the $\mathbf{q}_i$ must lie inside both Fermi spheres in Fig. 40. The resulting phase-space factor is $41/280\approx1/7$. Noting that diagram A7 has only three closed loops, and using (3.30) and (3.33), we find that (3.60) becomes

$$W(\mathrm{A7})\approx-\frac{1}{2}A^{-1}\frac{3}{16}\frac{1}{7}\frac{A^4}{4}\left(\frac{4\kappa}{3A}\right)^2\frac{4\bar{U}}{3A}=-\frac{\kappa^2\bar{U}}{126}. \tag{3.62}$$

Numerically we find $W(\mathrm{A7})\approx0.01$ MeV, which is so small that a more detailed calculation is pointless.

Class A8. To obtain a rough estimate for $W(\mathrm{A8})$, we omit the optional particle-particle interaction and use the same value of the reduction factor r as calculated for class A5. From (2.18) we get

$$W(\mathrm{A8})\approx-\tfrac{1}{2}A^{-1}(r/\bar{e})\sum\langle\zeta_{lm}\mid\zeta_{ij}-\zeta_{ji}\rangle \times\langle kn\mid G\mid lm\rangle\langle ij\mid G\mid kn\rangle, \tag{3.63}$$

where we have replaced the middle energy denominator of Fig. 17 by an appropriate average value $\bar{e}$. There is only one exchange diagram in addition to Fig. 17, and the statistical weight due to exchange is $1+(-\frac{1}{4})=\frac{3}{4}$. To calculate the phase-space factor, we use the variables

$$\mathbf{K}_1=\mathbf{l}+\mathbf{m}, \quad \mathbf{K}_2=\mathbf{k}+\mathbf{n}, \quad \mathbf{K}_3=\mathbf{i}+\mathbf{j},$$
$$\mathbf{q}_1=\tfrac{1}{2}(\mathbf{l}-\mathbf{m}), \quad \mathbf{q}_2=\tfrac{1}{2}(\mathbf{k}-\mathbf{n}), \quad \mathbf{q}_3=\tfrac{1}{2}(\mathbf{i}-\mathbf{j}). \tag{3.64}$$

Momentum conservation implies $\mathbf{K}_1=\mathbf{K}_2=\mathbf{K}_3$, and the discussion is now the same as for class A7. The phase-space factor is $41/280\approx\frac{1}{7}$. Four summations over the Fermi sea and two closed loops give a factor $\frac{1}{16}A^4$. Using (3.30) and (3.33) for the matrix elements in (3.63), we obtain

$$W(\mathrm{A8})\approx-\frac{1}{2}A^{-1}\frac{r}{\bar{e}}\frac{3}{4}\frac{1}{7}\frac{A^4}{16}\frac{4\kappa}{3A}\left(\frac{4\bar{U}}{3A}\right)^2=-\frac{r\kappa\bar{U}^2}{126\bar{e}}. \tag{3.65}$$

The energy denominator $\bar{e}$ involves the excitation of only two particles above the sea and is therefore somewhat smaller than the value $\bar{e}=530$ MeV calculated for class A5. If we take $\bar{e}=400$ MeV, formula (3.65) gives $W(\mathrm{A8})\approx-0.01$ MeV. This is so small that a better calculation is unnecessary.

Class A9. A rough estimate of $W(\mathrm{A9})$ can be made in the usual way. First, we rewrite (2.20) in the form

$$W(\mathrm{A9})=\tfrac{1}{2}A^{-1}\sum\langle\zeta_{kn}\mid\zeta_{lm}-\zeta_{ml}\rangle\langle\zeta_{lm}\mid\zeta_{ij}\rangle\langle ij\mid G\mid kn\rangle. \tag{3.66}$$

There is one exchange diagram in addition to Fig. 18, and the statistical weight is $\frac{3}{4}$. Using the variables (3.64), one finds a phase-space factor of $41/280\approx\frac{1}{7}$. Four summations over the Fermi sea and two closed loops give a factor $\frac{1}{16}A^4$. When we use (3.30) and (3.33), formula (3.66) becomes

$$W(\mathrm{A9})\approx\frac{1}{2}A^{-1}\frac{3}{4}\frac{1}{7}\frac{A^4}{16}\left(\frac{4\kappa}{3A}\right)^2\frac{4\bar{U}}{3A}=\frac{\kappa^2\bar{U}}{126}. \tag{3.67}$$

The value of (3.67) is $W(\mathrm{A9})\approx-0.01$ MeV, which is small enough to make a more detailed calculation unnecessary.

D. Three-Body Combination Diagrams

As was mentioned in Sec. III A, our numerical treatment of three-body combination diagrams is a crude one. Its main shortcoming is the omission of the tensor force in two important diagrams. The calculations are performed in coordinate space, and we therefore need coordinate-space representations for $\langle apq\mid Z_1\mid lmn\rangle$ and $\langle abc\mid Y\mid lmn\rangle$. In the reasonable

approximation of zero hole momenta, these coordinate-space amplitudes depend only on the three interparticle distances.[13] Thus we have

$$\langle \mathbf{r}_1\mathbf{r}_2\mathbf{r}_3 \mid Z_1 \mid lmn\rangle \rightarrow Z_1(r_{12}, r_{13}, r_{23}), \quad (3.68)$$

and a similar equation holds for Y. We use the approximate solution[12,13]

$$\begin{aligned} Z_1(r_{12}, r_{13}, r_{23}) &= \eta_{12}(1-\zeta_{13}+\tfrac{1}{2}\zeta_{13}\zeta_{23}) \\ &+\eta_{13}(1-\zeta_{12}+\tfrac{1}{2}\zeta_{12}\zeta_{23})-\eta_{23}(\zeta_{12}+\zeta_{13}-\zeta_{12}\zeta_{13}) \\ &+\zeta_{12}\zeta_{13}+\tfrac{1}{2}(\zeta_{12}+\zeta_{13})\zeta_{23}-\tfrac{4}{3}\zeta_{12}\zeta_{13}\zeta_{23}. \quad (3.69) \end{aligned}$$

Here, η_{12} means $\eta(r_{12})$ and ζ_{12} means $\zeta(r_{12})$. The corresponding approximation for Y is seen from (2.26) to be

$$Y(r_{12}, r_{13}, r_{23}) = \eta_{12}+\eta_{13}+\eta_{23}-\tfrac{1}{2}(Z_1+Z_2+Z_3). \quad (3.70)$$

In these formulas, $\eta(r)$ and $\zeta(r)$ represent the on-energy-shell and off-energy-shell two-body defect functions, respectively. For a two-body potential with a hard core, we have

$$\begin{aligned} \eta(r) &= 1, && r<c \\ &= \chi_L(k, r)/[rj_L(kc)], && r>c \quad (3.71) \end{aligned}$$

where an appropriate average over L and k must be taken, and χ_L is calculated on the energy shell. The same formula holds for $\zeta(r)$, but χ is then calculated off the energy shell, and the average value of k is larger. For our calculations with the Reid soft-core potential, we have simply put $c=0$ in (3.71) and have used (3.69) (which was derived for a potential with a hard core). It has been pointed out[13] that this is not the best way to handle a soft-core potential. It would probably be better to define some effective core radius of about 0.3–0.4 F for the soft-core potential. Nevertheless, the present rough treatment should give results of the right order of magnitude (for central forces). So we expect to learn which of the three-body combination diagrams are important and which are negligible.

In order to obtain $\eta(r)$ from (3.71), we calculated $\chi_0(k, r)$ for the average relative momentum $k=(0.3)^{1/2}k_F=0.745$ F^{-1} of occupied states. The Reid $^1S_0$ soft-core potential was used. We took $K=2k$, and

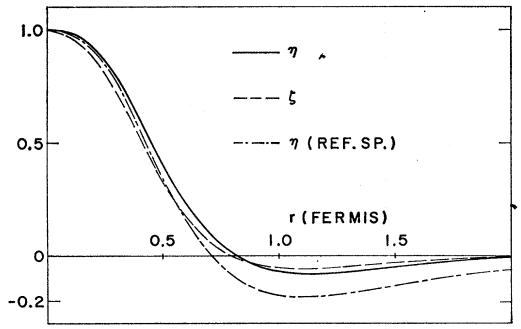

FIG. 44. Dimensionless functions $\eta(r)$ and $\zeta(r)$. The dot-dash curve is the reference-spectrum approximation for $\eta(r)$.

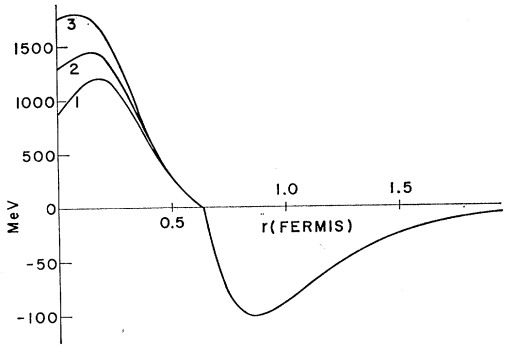

FIG. 45. The effective interaction $g(r)$ for three different choices of k, γ^2. Curve 1: $k=1.4$ F^{-1}, $\gamma^2=8.88$ F^{-2}. Curve 2: $k=1.8$ F^{-1}, $\gamma^2=12.72$ F^{-2}. Curve 3: $k=2.2$ F^{-1}, $\gamma^2=17.52$ F^{-2}. The total momentum K was 2.7 F^{-1} in all cases. The three curves coincide for $r>0.65$ F. Note the different vertical scales used above and below the horizontal axis.

γ^2 was found from (3.25) to be 2.61 F^{-2}. The resulting function $\eta(r)$ is plotted in Fig. 44.

The best values of k, K to be used in calculating $\zeta(r)$ have been derived by Kirson.[13] He finds $k=0.56/c$ and $K=1.1/c$. For a core radius $c=0.4$ F, one finds $k=1.4$ F^{-1}, $K=2.75$ F^{-1}, and we used these values. The off-energy-shell value of γ^2 must reproduce the excitation energy of three particles above the Fermi sea.[2,13,14] Thus we have

$$e=k_{ab}^2+\gamma_3^2=k_{ab}^2+\tfrac{1}{4}K_{ab}^2+\tfrac{1}{2}c^2-E(l)-E(m)-E(n), \quad (3.72)$$

where the subscript on γ_3^2 reminds us that three particles are above the sea. The sum of three hole energies is replaced by $3\bar{E}$, where $\bar{E}=-43$ MeV. The total momentum of all three particles will tend to be small, and we assume it is zero. Then the momentum c of the spectator particle is equal to K_{ab}, and we find

$$\gamma_3^2=\tfrac{3}{4}K_{ab}^2-3\bar{E}=8.78 \text{ F}^{-2}. \quad (3.73)$$

The slightly different value of 8.47 F^{-2} was actually used in the calculations. The Reid $^1S_0$ soft-core potential was used, and the resulting function $\zeta(r)$ is shown in Fig. 44.

A further approximation[13,14] that is made here is to replace certain off-energy-shell G matrices, such as the one in (2.25), by a local function $g(r)$. Bethe[11] has shown how to improve on this approximation, but the use of his improved method is not worthwhile in our already rough calculations. The function $g(r)$ is defined by

$$g(r)=v(r)u_L(k, r)/[rj_L(kr)], \quad (3.74)$$

where an appropriate average over k and L must be used. Matrix elements of $g(r)$ between *unperturbed* plane waves will be approximately equal to the corresponding matrix elements of G.

We calculated $g(r)$ from (3.74) with the $^1S_0$ Reid soft-core potential. The appropriate average values of k, K are given by Kirson as $k=0.72/c=1.8$ F^{-1}, $K=$

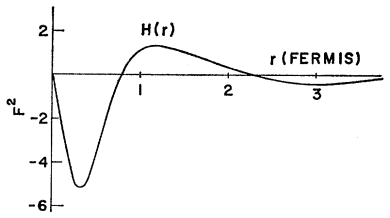

FIG. 46. Function $H(r)$ that arises in the calculation of $W(\mathrm{B1})$.

$1.44/c=3.6$ F^{-1}, where $c=0.4$ F. The value of γ^2 is then found from (3.73) to be 12.84 F^{-2}. The resulting function $g(r)$ is plotted in Fig. 45. The average values of k, K used here were derived by Kirson for use in expression (2.25), which arises in the calculation of W_3. The best values of k, K may be different for G matrices in other types of diagrams. Such cases will be discussed as they arise. We have found that $g(r)$ is insensitive to k, K, γ^2 for $r>0.5$ F. For smaller r, the repulsion increases as γ^2 becomes larger.

Class B1. In our approximation of spin-independent central forces and small hole momenta, all exchange diagrams are included by multiplying the direct diagram by the proper statistical weight. Referring to Fig. 22, we see that permuting the hole lines l, m, and n at the bottom of the diagram gives six diagrams with a total statistical weight of $1+3\times(-\frac{1}{4})+2\times\frac{1}{16}=\frac{3}{8}$. The remaining exchange diagrams are now obtained by permuting the hole lines l, m, and k at the top of the diagram. However, exchange of l, m at both top and bottom leaves the diagram unchanged. So, for each permutation of l, m, and n at the bottom, there are just three permutations of l, m, and k at the top. These are the identity, the exchange of l and k, and the exchange of m and k. The resulting statistical weight is $1+2\times(-\frac{1}{4})=\frac{1}{2}$. Thus we finally obtain $\frac{1}{2}\times\frac{3}{8}=\frac{3}{16}$ for the statistical weight of the whole diagram.

We omit the optional particle-particle interaction for the present. Multiplying the direct term by $\frac{3}{16}$ gives, according to (2.27) [the statistical weight $\frac{3}{16}$ already contains the factor $\frac{1}{2}$ that appears in (2.27)],

$$W_1(\mathrm{B1})=-A^{-1}\tfrac{3}{16}\sum\langle lmk\mid Z_1{}^{\dagger}G_{23}\mid abk\rangle$$
$$\times(E_a+E_b-E_l-E_m)^{-1}\langle abn\mid G_{13}Z_2+G_{23}Z_1\mid lmn\rangle, \quad (3.75)$$

where the subscript on W_1 indicates that the particle-particle interaction is omitted. Using the approximation of zero hole momenta, and putting the G matrix equal to a local function of r, we can easily evaluate the three-body matrix elements. For example, we find

$$\langle abn\mid G_{13}Z_2\mid lmn\rangle=\Omega^{-2}\int\exp(-i\mathbf{k}\cdot\mathbf{r}_{12})\,g(r_{13})$$
$$\times Z_2(r_{12},r_{13},r_{23})\,d\tau_3\,d\tau_{12}, \quad (3.76)$$

where $\mathbf{k}=\frac{1}{2}(\mathbf{a}-\mathbf{b})$ is the relative momentum of a, b.

The summation over $lmnk$ simply gives a factor A^4. In summing over a, b we note that the total momentum $\mathbf{a}+\mathbf{b}$ is fixed at zero by momentum conservation. But the sum over the relative momentum $\mathbf{k}$ gives $\Omega(2\pi)^{-3}\int d^3k\ Q(k)$, where $Q(k)$ requires that $k>k_F$. The energy denominator $E_a+E_b-E_l-E_m$ is equal to $k^2+\gamma^2$, where γ^2 takes its on-energy-shell value of 2.61 F^{-2}.

Putting all these results together, we find

$$W_1(\mathrm{B1})\approx-\tfrac{3}{8}\rho^3\int\frac{d^3k}{(2\pi)^3}\,k^{-1}H(k)\,\frac{Q(k)}{k^2+\gamma^2}\,k^{-1}H(k), \quad (3.77)$$

$$H(k)=4\pi k\int_0^\infty rj_0(kr)H(r)\,dr, \quad (3.78)$$

$$H(r_{12})=r_{12}\int g(r_{13})Z_2(r_{12},r_{13},r_{23})\,d\tau_3$$
$$=r_{12}\int g(r_{23})Z_1(r_{12},r_{13},r_{23})\,d\tau_3. \quad (3.79)$$

The equality of the two expressions in (3.79) follows from invariance of $H(r_{12})$ under interchange of 1 and 2 and from the symmetry property

$$Z_1(r_{12},r_{13},r_{23})=Z_2(r_{12},r_{23},r_{13}). \quad (3.80)$$

This last equation can be checked directly from (3.69). A more general discussion is given by Kirson.[13] Thus, under our approximations, the two terms in (3.75) are equal. Note also that the appropriate values of k, K, γ^2 to be used in calculating $g(r)$ are exactly the same as in a three-body cluster diagram.

The optional particle-particle interaction is included simply by inserting a minus sign in (3.77) and replacing one of the factors $H(k)$ by

$$H_D(k)=4\pi k\int_0^\infty\chi_0(k,r)H(r)\,dr. \quad (3.81)$$

Here $\chi_0(k,r)$ is calculated on the energy shell with $\gamma^2=2.61$ F^{-2}.

The function $H(r)$ is plotted in Fig. 46, and $H(k)$ and $H_D(k)$ are plotted in Fig. 47. The contribution obtained from (3.77) without the particle-particle interaction is -0.69 MeV. But the contribution including the particle-particle interaction cancels 62% of this, leaving a final result of $W(\mathrm{B1})=-0.26$ MeV.

It is reasonable to expect the inclusion of the tensor force to enhance the size of $W(\mathrm{B1})$ considerably. The Reid $^1S_0$ potential, acting only in S waves, gives $\kappa=0.044$. But the contribution to κ from the D state

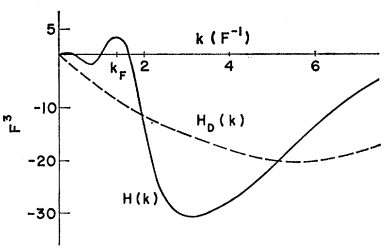

FIG. 47. Functions $H(k)$ and $H_D(k)$ that are needed in the calculation of $W(\mathrm{B1})$.

induced by the tensor force is 0.067. Hence including the tensor force will make κ about 2.5 times larger. If $W(\mathrm{B1})$ were to scale as κ^2, we would then obtain six times as large a result when the tensor force was included. This is probably an overstimate because the tensor force flips the spin, and the orthogonality of different spin states may reduce the tensor-force contribution to the three-body amplitudes.

There is another factor that favors the tensor force here. The tensor force will probably give much less cancellation between the terms with and without the optional particle-particle interaction. We have already seen by explicit calculation in Sec. III A that this is the case for class A5.

A reliable estimate of the effect of the tensor force will require a detailed study. But it seems reasonable to expect the inclusion of the tensor force in $W(\mathrm{B1})$ to give a good fraction of an MeV of additional binding. Thus we want to direct attention to the diagrams of class B1. Of all the four-hole-line diagrams, it is this class that most deserves further study.

Class B2. We use the ideas explained in Sec. III B to obtain a rough estimate of $W(\mathrm{B2})$. We note first that all exchange diagrams are obtained by permuting the hole lines *lkn* at the bottom of Fig. 26(a). Thus the statistical weight due to exchange is found to be $\frac{3}{8}$. Next we note that the momentum $\mathbf{c}=\mathbf{k}+\mathbf{n}-\mathbf{m}$ cannot be very large. Hence the matrix element $\langle kn \mid G \mid mc\rangle$, which appears in formula (2.29) for $W(\mathrm{B2})$, involves only states of fairly low momentum and is approximated by $\frac{4}{3}\bar{U}A^{-1}$ according to (3.33).

Since the direct diagram has three closed loops, the sum over *lmnk* gives a factor $\frac{1}{4}A^4$. The requirement that $|\mathbf{c}|=|\mathbf{k}+\mathbf{n}-\mathbf{m}|>k_F$ gives a phase-space factor. This phase-space factor is one minus the phase-space factor for the hole-hole diagram and is therefore equal to $\frac{2}{3}$.

For simplicity in the evaluation of $\langle abc \mid Y \mid lkn\rangle$ [which appears in formula (2.29) for $W(\mathrm{B2})$] we take $\mathbf{l}+\mathbf{k}+\mathbf{n}=0$ so that $\mathbf{a}+\mathbf{b}\equiv\mathbf{K}_{ab}=-\mathbf{c}$. Then we find

$$\langle abc \mid Y \mid lkn\rangle=\Omega^{-2}\int \exp(-i\mathbf{k}\cdot\mathbf{r}_{12})\,d\tau_{12}$$
$$\times\int \exp[-i\mathbf{c}\cdot(\mathbf{r}_3-\mathbf{R}_{12})]\,Y(r_{12}, r_{13}, r_{23})\,d\tau_3, \quad (3.82)$$

where $\mathbf{k}$ is the relative momentum of a, b. We can also write

$$\langle lm \mid G(Q/e) \mid ab\rangle=\Omega^{-1}\int\eta(r)\,\exp(i\mathbf{k}\cdot\mathbf{r})\,d\tau. \quad (3.83)$$

When (3.82) and (3.83) are now multiplied together, and the sum over ab is replaced by $\Omega(2\pi)^{-3}\int d^3k$, the k-space integral gives a δ function that simplifies the spatial integrations.

One more simplification is to replace the second plane wave in (3.82) by its S-wave part. This is a good approximation because $|\mathbf{c}|$ is not very large, and $Y(r_{12}, r_{13}, r_{23})$ goes rapidly to zero when $|\mathbf{r}_3-\mathbf{R}_{12}|$ becomes large. Putting all our results together, we obtain from (2.29)

$$W(\mathrm{B2})=\tfrac{1}{6}\bar{U}\rho^2\int\eta(r_{12})\,L(r_{12})\,d\tau_{12}, \quad (3.84)$$
$$L(r_{12})=\int j_0(c\mid \mathbf{r}_3-\mathbf{R}_{12}\mid)\,Y(r_{12}, r_{13}, r_{23})\,d\tau_3. \quad (3.85)$$

Expression (3.84) was evaluated for $c=1.5k_F$, $c=2.0k_F$, and $c=2.5k_F$. The results were -0.07, -0.12, and -0.08 MeV, respectively. So a reasonable average value is $W(\mathrm{B2})=-0.1$ MeV.

Inclusion of the tensor will make the functions η and Y larger. Hence the magnitude of $W(\mathrm{B2})$ could become several times larger than our estimate of -0.1 MeV. For this reason, class B2 is worthy of further study in which the tensor force is properly taken into account.

Class B3. The sum over a, b in (2.30) can be performed by closure to obtain an expression containing κ_{lm}, as defined by (3.14). Neglecting the dependence of κ_{lm} on the momenta of l and m, and using (2.22) and (3.37), we find that (2.30) becomes

$$W(\mathrm{B3})=-3\kappa W_3, \quad (3.86)$$

where W_3 is the energy per particle from three-body clusters. Assuming that W_3 has been accurately evaluated, formula (3.86) is very accurate and includes all effects of the tensor force. The numerical value of (3.86) is $W(\mathrm{B3})=+0.45$ MeV.

Class B4. We make a rough estimate of $W(\mathrm{B4})$, using the methods discussed in Sec. III B. When the sum over ab is carried out in (2.32), the factor outside the square brackets becomes $\langle\zeta_{lm}\mid\zeta_{kn}\rangle$, which we replace by $\frac{4}{3}\kappa A^{-1}$. This matrix element requires that the spins and isospins of l, m be equal, respectively, to those of k, n. Therefore, since the two-body defect function $\chi_0(k_0, r)$ is nearly independent of the relative momentum k_0, we have

$$\langle kn \mid G(Q/e) \mid ef\rangle\approx\langle ml \mid G(Q/e) \mid fe\rangle.$$

This in turn allows us to write

$$\sum_{efpq}\langle kn \mid G(Q/e) \mid ef\rangle\langle ej \mid G \mid pq\rangle$$
$$\times\langle fpq \mid Z_1{}^A \mid mlj\rangle\approx W_3/A^2, \quad (3.87)$$

where W_3 is given by (2.22) and (2.23). The same argument shows that each of the other two terms inside the square brackets of (2.32), when summed over *efpq*, is also approximately equal to W_3/A^2. Since the direct diagram has three closed loops, the sum over occupied states gives a factor $\frac{1}{4}A^4$. Finally, there is a phase-space of $\frac{1}{3}$ that is the same as for the hole-hole diagram. So our estimate is

$$W(\mathrm{B4})\approx A^{-1}\frac{4\kappa}{3A}\frac{3W_3}{A^2}\frac{A^4}{4}\frac{1}{3}=\frac{1}{3}\kappa W_3. \quad (3.88)$$

Numerically we find $W(\mathrm{B4})\approx-0.05$ MeV. The tensor force is included here, at least in an average way, by

our use of the correct values of κ and W_3. Our estimate for $W(\mathrm{B4})$ is sufficiently small that a more accurate calculation seems unnecessary.

Class B5. Assuming spin-independent central forces and small hole momenta, we make a rough estimate of $W(\mathrm{B5})$ along the lines of Sec. III B. All exchange diagrams are obtained by permuting the hole lines *knj* at the bottom of Fig. 30. Hence exchange is taken into account by multiplying the direct diagram by a statistical weight of $\frac{3}{8}$. Also, just as in the hole-hole diagram, there is a phase-space factor of $\frac{1}{3}$.

The matrix element $\langle kn \mid G \mid lm\rangle$ in (2.33) is approximated by $\frac{4}{3}\bar{U}A^{-1}$. We also find

$$\sum_{abc}\langle lmj \mid Y^{\dagger} \mid abc\rangle\langle abc \mid Y \mid knj\rangle \approx \Omega^{-2} \times \int [Y(r_{12}, r_{13}, r_{23})]^2 d\tau_2\, d\tau_3. \quad (3.89)$$

Since the direct diagram has three closed loops, the sum over occupied states gives a factor $\frac{1}{4}A^4$.

Combining the factors mentioned above with the factor $\frac{1}{2}A^{-1}$ that already appears in (2.33), we obtain

$$W(\mathrm{B5}) \approx (1/48)\bar{U}\rho^2 \int [Y(r_{12}, r_{13}, r_{23})]^2 d\tau_2\, d\tau_3. \quad (3.90)$$

Numerical evaluation of this expression gives $W(\mathrm{B5}) \approx -0.02$ MeV. This calculation includes only the ${}^1S_0$ potential. If (3.90) scales as κ^2, then including the tensor force will increase $W(\mathrm{B5})$ by about a factor of 6 [see our discussion of $W(\mathrm{B1})$]. However, it seems unlikely that an accurate calculation of $W(\mathrm{B5})$ would give more than about 0.1 MeV of binding.

Class B6. Omitting for the moment the optional particle-particle interaction, we make a rough estimate, assuming spin-independent central forces and small hole momenta. In formula (2.35) we replace $E_c + E_d - E_l - E_m$ by an average energy denominator $\bar{e}$. The approximate value $\frac{4}{3}\bar{U}A^{-1}$ is used for the matrix element $\langle lm \mid G \mid kn\rangle$. This matrix element requires that the spins and isospins of l, m be equal, respectively, to those of k, n. The argument that was used for class B4 now shows that $\langle kn \mid G(Q/e) \mid cd\rangle$, when combined with the first term inside the brackets of (2.35) and summed over *cdpq*, is approximately equal to W_3/A^2. The sum over occupied states gives a factor $\frac{1}{4}A^4$. As in the hole-hole diagram, there is a phase space factor of $\frac{1}{3}$. Formula (2.35) only accounts for Fig. 31(a), whose contribution differs from that of Fig. 31(b) by the replacement $\langle lm \mid G(kn) \mid kn\rangle \rightarrow \langle lm \mid G(lm) \mid kn\rangle$. This difference in starting energy is numerically unimportant, and we can therefore include Fig. 31(b) by inserting a factor of 2. Putting these results together, and inserting a reduction factor r to account for the particle-particle interaction, we get

$$W(\mathrm{B6}) \approx -(2/9)(r\bar{U}/\bar{e})W_3. \quad (3.91)$$

The value of r is uncertain, but we will undoubtedly overestimate the magnitude of $W(\mathrm{B6})$ if we put $r=1$. Taking $\bar{e}=400$ MeV then gives $W(\mathrm{B6}) \approx -0.04$ MeV. The effect of the tensor force is largely included by our use of values of $\bar{U}$ and W_3 that contain the effects of the tensor force. The small value of $W(\mathrm{B6})$ means that a more accurate calculation is not necessary.

E. Four-Body Cluster Diagrams

In our treatment of four-body clusters, we make the same approximations as for the three-body combination diagrams. Thus we put all hole momenta equal to zero, omit the tensor force, and approximate the G matrix by a local function of r. We will first use these approximations to replace formula (2.41) for W_4 by an approximate formula that is useful for computation. Next we derive an approximate solution of the four-body Bethe-Faddeev equations, using a method[12] developed previously for the three-body Bethe-Faddeev equations. Finally, this approximate solution is used to evaluate the approximate formula for W_4 numerically.

Before making any approximations, we rewrite (2.41) as an integral over coordinate space in the form

$$W_4 = \tfrac{1}{2}A^{-1}\sum_{lmnk}\int d\mathbf{r}_1\, d\mathbf{r}_2\, d\mathbf{r}_3\, d\mathbf{r}_4 \times [\langle ln \mid G(Q/e) \mid \mathbf{r}_1\mathbf{r}_3\rangle\langle mk \mid G(Q/e) \mid \mathbf{r}_2\mathbf{r}_4\rangle + \langle lmn \mid Y^{\dagger} \mid \mathbf{r}_1\mathbf{r}_2\mathbf{r}_3\rangle\langle k \mid \mathbf{r}_4\rangle] \times G_{34}\langle \mathbf{r}_1\mathbf{r}_2\mathbf{r}_3\mathbf{r}_4 \mid C_{34}{}^A \mid lmnk\rangle. \quad (3.92)$$

Here, $\langle k \mid \mathbf{r}_4\rangle$ is the single-particle plane wave $\phi_k{}^*(\mathbf{r}_4)$, and G_{34} is the off-energy-shell G-matrix operator acting on $\mathbf{r}_3$ and $\mathbf{r}_4$. The integrand of (3.92) carries a normalization factor Ω^{-4}. However, the last spatial integral is trivial and simply gives a factor Ω. So, when we rewrite formula (3.92) below, we will include only three spatial integrations and insert a normalization factor Ω^{-3}.

We now make the approximation of zero hole momenta. Thus the integrand of (3.92) is independent of *lmnk*, and the sum over these occupied states simply gives a factor A^4. Also, $\langle k \mid \mathbf{r}_4\rangle$ becomes unity times a normalization factor $\Omega^{-1/2}$. And all other wave functions in (3.92) depend only on the interparticle distances, e.g.,

$$\langle \mathbf{r}_1\mathbf{r}_2\mathbf{r}_3\mathbf{r}_4 \mid C_{34} \mid lmnk\rangle \rightarrow C_{34}(r_{12}, r_{13}, r_{14}, r_{23}, r_{24}, r_{34}). \quad (3.93)$$

Further, we replace G_{34} by $g(r_{34})$.

We include exchange diagrams in the usual way by multiplying the direct diagram by an appropriate statistical weight. Permuting the hole lines *lmnk* at the bottom of a four-body cluster diagram gives 23 exchange diagrams in addition to the direct diagram. The total statistical weight is found to be $1+6\times(-\frac{1}{4})+11\times(\frac{1}{16})+6\times(-\frac{1}{64})=\frac{3}{32}$. This factor can also be deduced from the following physical argument. If all hole momenta are zero, the unperturbed four-

body wave function is completely symmetric in the spatial variables. Hence it must be completely antisymmetric in spin-isospin variables. The fraction of four-particle states that is completely antisymmetric in spin and isospin is easily seen to be 3/32. It is interesting to note that the corresponding statistical weight for five-particle states is zero, i.e., there is no five-particle state that is completely antisymmetric in spin and isospin. Thus the five-body cluster diagrams would contribute nothing in the approximation of zero hole momenta.

Putting our results together, we can rewrite (3.92) in the form

$$W_4=(3/32)\rho^3\int D(r_{34})\,g(r_{34})\,d\tau_{34}, \tag{3.94}$$

$$D(r_{34})=\tfrac{1}{2}\int d\tau_1\,d\tau_2[\eta(r_{13})\eta(r_{24})+Y(r_{12},r_{13},r_{23})] \times C_{34}(r_{12},r_{13},r_{14},r_{23},r_{24},r_{34}). \tag{3.95}$$

These two formulas are the ones we actually use for computation. But before doing this, we must obtain an approximate expression for the four-body wave function C_{34}.

In the four-body Bethe-Faddeev equations (2.40), we put the momenta of the hole states *lmnk* equal to zero, in accord with the discussion above. Changing from the $\langle abpq\,|$ representation to the $\langle \mathbf{r}_1\mathbf{r}_2\mathbf{r}_3\mathbf{r}_4\,|$ representation then gives

$$\begin{aligned}C_{34}(r_{12},r_{13},r_{14},r_{23},r_{24},r_{34})&=\eta(r_{13})\eta(r_{24})+\eta(r_{14})\eta(r_{23})\\&+Y(r_{12},r_{13},r_{23})+Y(r_{12},r_{14},r_{24})-(Q_{12}/e)G_{12}C_{12}\\&-(Q_{13}/e)G_{13}C_{13}-(Q_{14}/e)G_{14}C_{14}\\&-(Q_{23}/e)G_{23}C_{23}-(Q_{24}/e)G_{24}C_{24}.\end{aligned} \tag{3.96}$$

The reaction matrices G_{ij} are calculated off the energy shell, with the starting energy involving the excitation energy of four particles above the Fermi sea.

We now introduce the approximation of Ref. 12 for the operator $(Q_{ij}/e)G_{ij}$ to obtain

$$\begin{aligned}C_{34}=\eta_{13}\eta_{24}+\eta_{14}\eta_{23}+Y_{123}+Y_{124}-\zeta_{12}C_{12}\\-\zeta_{13}C_{13}-\zeta_{14}C_{14}-\zeta_{23}C_{23}-\zeta_{24}C_{24}.\end{aligned} \tag{3.97}$$

Here we define

$$\begin{aligned}&\zeta_{13}C_{13}(r_{12},r_{13},r_{14},r_{23},r_{24},r_{34})\\&\quad=\zeta(r_{13})C_{13}(r_{12},r_{13},r_{14},r_{23},r_{24},r_{34}), \qquad r_{13}\le c\\&\quad=\zeta(r_{13})C_{13}(r_{12},c,r_{14},r_{23},r_{24},r_{24}), \qquad r_{13}>c\end{aligned} \tag{3.98}$$

where c is the radius of an assumed hard core. Similar formulas hold for the other terms in (3.97) that have the same structure as $\zeta_{13}C_{13}$. As was discussed in connection with (3.71), $\eta(r)$ and $\zeta(r)$ are the two-body defect functions calculated on the energy shell and off the energy shell, respectively. From (3.68) and (3.69), we find

$$\begin{aligned}Y_{123}=\eta_{12}(\zeta_{13}+\zeta_{23}-\zeta_{13}\zeta_{23})+\eta_{13}(\zeta_{12}+\zeta_{23}-\zeta_{12}\zeta_{23})\\+\eta_{23}(\zeta_{12}+\zeta_{13}-\zeta_{12}\zeta_{13})-\zeta_{12}\zeta_{13}-\zeta_{12}\zeta_{23}-\zeta_{13}\zeta_{23}\\+2\zeta_{12}\zeta_{13}\zeta_{23}.\end{aligned} \tag{3.99}$$

The starting energies for the ζ's in (3.99) and (3.98) involve the excitation of three and four particles above the sea, respectively. We follow Lawson and Sampanthar[31] and Kuriyama[32] by representing both of these ζ's by the same function. This simplifies the formulas and is a good approximation because $\zeta(r)$ is not very sensitive to the starting energy.

Equation (3.97) is just one of six coupled equations for the C_{ij}. These equations can be solved analytically to obtain an approximate solution for C_{12} as a polynomial in the two-body functions $\eta(r)$ and $\zeta(r)$.

In solving (3.97), we make extensive use of the fact that if r_{ij} and r_{kl} are both less than c, then $C_{ij}=C_{kl}$. (The pairs ij and kl are different but may have one index in common, e.g., $ij=23$ and $kl=34$.) This symmetry property does *not* hold for the exact four-body wave function C_{12}. But it holds for the solution of the approximate Eq. (3.97) because of our approximation (3.98) for the effect of the operator $(Q/e)G$ on a four-body wave function. To see this, consider the diagrams that contribute to C_{ij} and C_{kl}. Those in which the last interaction is neither ij nor kl are common to C_{ij} and C_{kl}. There is a 1-1 correspondence between the C_{ij} diagrams with last interaction kl and the C_{kl} diagrams with last interaction ij. (Replacing each ij interaction by kl, and vice versa, takes one class of diagrams into the other.) Consider two corresponding diagrams, and assume that $r_{ij}<c$ and $r_{kl}<c$. Then, using (3.98) for the effect of $(Q/e)G$ on a four-body function, one can easily see that the two corresponding diagrams give equal contributions. Thus our basic approximation for the operator $(Q/e)G$ enforces the symmetry property that $C_{ij}=C_{kl}$ whenever r_{ij} and r_{kl} are both less than c.

We can now solve Eqs. (3.97). Suppose first that all r_{ij} are less than c. Then the C_{ij} are all equal, and $\eta_{ij}=\zeta_{ij}=1$, $Y_{ijk}=2$. Equation (3.97) gives $C_{12}=6-5C_{12}$, which implies $C_{12}=1$. Next we take $r_{12}>c$ and all other $r_{ij}<c$. According to the symmetry property discussed above, all the C_{ij} are equal except that C_{12} differs from the others. Thus it is sufficient to solve for C_{12} and C_{13}. In the equation of type (3.97) for C_{13}, there occurs on the right-hand side the term $\zeta_{12}C_{12}$. In this term, C_{12} is evaluated for all $r_{ij}<c$, and therefore has the value 1, according to our previous calculation. Using (3.99), we then obtain from (3.97)

$$\begin{aligned}C_{12}&=6-5C_{13},\\C_{13}&=4+2\eta_{12}-\zeta_{12}-4C_{13},\end{aligned} \tag{3.100}$$

which has the solution

$$C_{12}=2-2\eta_{12}+\zeta_{12},$$
$$C_{13}=\tfrac{1}{5}(4+2\eta_{12}-\zeta_{12}). \quad (3.101)$$

Having obtained the solution when one of the r_{ij} is larger than c, we can next consider cases in which two of the r_{ij} are larger than c. This process is continued step by step until the solution is obtained for all $r_{ij}>c$. In each step, many of the C_{ij} on the right-hand side of (3.97) will be known from the solutions obtained in earlier steps. The algebra is straightforward but tedious, and the final result is

$$\begin{aligned}C_{12}=\eta_{12}\{&-(\zeta_{13}+\zeta_{23})(\zeta_{14}+\zeta_{24})+\zeta_{13}\zeta_{14}(\zeta_{23}+\zeta_{24})+\zeta_{23}\zeta_{24}(\zeta_{13}+\zeta_{14})-\zeta_{13}\zeta_{14}\zeta_{23}\zeta_{24}\}\\
&+\eta_{13}\{\zeta_{14}+\zeta_{34}-\tfrac{1}{2}\zeta_{12}(\zeta_{14}+\zeta_{24}+\zeta_{34})-\zeta_{14}\zeta_{23}-\zeta_{14}\zeta_{34}-\zeta_{23}\zeta_{34}\\
&+\zeta_{12}(\zeta_{14}+\zeta_{34})[(5/6)\zeta_{23}+\tfrac{1}{6}\zeta_{24}]+\tfrac{1}{3}\zeta_{12}(\zeta_{14}\zeta_{34}+\zeta_{23}\zeta_{24})+\zeta_{14}\zeta_{23}\zeta_{34}\\
&-\tfrac{1}{6}\zeta_{12}\zeta_{23}\zeta_{24}(\zeta_{14}+\zeta_{34})-\tfrac{3}{4}\zeta_{12}\zeta_{14}\zeta_{23}\zeta_{34}+(1/15)\zeta_{12}\zeta_{14}\zeta_{23}\zeta_{24}\zeta_{34}\}+\eta_{23}\{\ \}+\eta_{14}\{\ \}+\eta_{24}\{\ \}\\
&+\eta_{34}\{(\zeta_{13}+\zeta_{14}+\zeta_{23}+\zeta_{24})(1+\tfrac{1}{2}\zeta_{12})-\zeta_{13}\zeta_{14}-\zeta_{13}\zeta_{23}-\zeta_{13}\zeta_{24}-\zeta_{14}\zeta_{23}\\
&-\zeta_{14}\zeta_{24}-\zeta_{23}\zeta_{24}+\zeta_{13}\zeta_{14}(\zeta_{23}+\zeta_{24})+\zeta_{23}\zeta_{24}(\zeta_{13}+\zeta_{14})-\tfrac{1}{3}\zeta_{12}(\zeta_{13}+\zeta_{14})(\zeta_{23}+\zeta_{24})\\
&-\tfrac{2}{3}\zeta_{12}(\zeta_{13}\zeta_{14}+\zeta_{23}\zeta_{24})+\tfrac{1}{3}\zeta_{12}\zeta_{13}\zeta_{14}(\zeta_{23}+\zeta_{24})+\tfrac{1}{3}\zeta_{12}\zeta_{23}\zeta_{24}(\zeta_{13}+\zeta_{14})-\zeta_{13}\zeta_{14}\zeta_{23}\zeta_{24}-(4/15)\zeta_{12}\zeta_{13}\zeta_{14}\zeta_{23}\zeta_{24}\}\\
&+\eta_{12}\eta_{34}\{(1-\zeta_{13})(1-\zeta_{14})(1-\zeta_{23})(1-\zeta_{24})-1\}+\eta_{13}\eta_{24}\{1-(1-\tfrac{1}{2}\zeta_{12})(\zeta_{14}+\zeta_{23}+\zeta_{34})\\
&+(1-\tfrac{2}{3}\zeta_{12})(\zeta_{14}\zeta_{23}+\zeta_{14}\zeta_{34}+\zeta_{23}\zeta_{34})-\zeta_{14}\zeta_{23}\zeta_{34}+\tfrac{3}{4}\zeta_{12}\zeta_{14}\zeta_{23}\zeta_{34}\}\\
&+\eta_{14}\eta_{23}\{\ \}-[\zeta_{13}\zeta_{14}+\zeta_{13}\zeta_{34}+\zeta_{14}\zeta_{34}+\zeta_{23}\zeta_{24}+\zeta_{23}\zeta_{34}+\zeta_{24}\zeta_{34}]\\
&+\zeta_{13}\zeta_{14}(\zeta_{23}+\zeta_{24}+2\zeta_{34})+\zeta_{23}\zeta_{24}(\zeta_{13}+\zeta_{14}+2\zeta_{34})+2\zeta_{34}(\zeta_{13}\zeta_{23}+\zeta_{14}\zeta_{24})\\
&+\zeta_{34}(\zeta_{13}\zeta_{24}+\zeta_{14}\zeta_{23})+\tfrac{4}{3}\zeta_{12}(\zeta_{13}+\zeta_{23})(\zeta_{14}+\zeta_{24})+\tfrac{1}{3}\zeta_{12}\zeta_{34}(\zeta_{13}+\zeta_{14}+\zeta_{23}+\zeta_{24})\\
&-\zeta_{13}\zeta_{14}\zeta_{23}\zeta_{24}-\tfrac{3}{2}\zeta_{12}\zeta_{34}(\zeta_{13}\zeta_{23}+\zeta_{14}\zeta_{24})-\tfrac{1}{2}\zeta_{12}\zeta_{34}(\zeta_{13}\zeta_{14}+\zeta_{23}\zeta_{24})-\tfrac{3}{4}\zeta_{12}\zeta_{34}(\zeta_{13}\zeta_{24}+\zeta_{14}\zeta_{23})\\
&-2(\zeta_{23}+\zeta_{24})(\zeta_{12}+\zeta_{34})\zeta_{13}\zeta_{14}-2(\zeta_{13}+\zeta_{14})(\zeta_{12}+\zeta_{34})\zeta_{23}\zeta_{24}+(32/15)\zeta_{12}\zeta_{13}\zeta_{14}\zeta_{23}\zeta_{24}+22\zeta_{12}\zeta_{34}(\zeta_{13}\zeta_{14}\zeta_{23}\\
&+\zeta_{13}\zeta_{14}\zeta_{24}+\zeta_{13}\zeta_{23}\zeta_{24}+\zeta_{14}\zeta_{23}\zeta_{24})/15+2\zeta_{13}\zeta_{14}\zeta_{23}\zeta_{24}\zeta_{34}-(5/3)\zeta_{12}\zeta_{13}\zeta_{14}\zeta_{23}\zeta_{24}\zeta_{34}. \quad (3.102)\end{aligned}$$

In this formula, the coefficient of η_{23} is obtained from the coefficient of η_{13} by everywhere interchanging the indices 1 and 2. Analogous statements hold for the coefficients of η_{14}, η_{24}, and $\eta_{14}\eta_{23}$.

Formula (3.102) is analogous to the approximate solution (3.69) of the three-body Bethe-Faddeev equations. In the three-body case,[12] it was found that the total three-body wave function, in the special case $\zeta\to\eta$, was equal to $(1-\eta_{12})(1-\eta_{13})(1-\eta_{23})$. This expression had been suggested earlier by Moszkowski,[38] and it gives the same type of correlations as are assumed in the Jastrow method.[39] It is of interest to see whether our formula for the four-body function C_{12} leads to a similar connection with the Jastrow method.

The total four-body wave function Ψ is defined by

$$\Psi=1-\sum_{\text{pairs}}\eta_{ij}+\tfrac{1}{5}[\eta_{12}\eta_{34}+\eta_{13}\eta_{24}+\eta_{14}\eta_{23}+2(Y_{123}+Y_{124}+Y_{134}+Y_{234})+\sum_{\text{pairs}}C_{ij}]. \quad (3.103)$$

The first term is the product of four unperturbed plane waves in the limit of zero momentum. The second term represents the six ways in which a pair of particles can scatter out of the Fermi sea, with no other interactions taking place. When terms from the C_{ij} are included, (3.103) is seen to contain three terms of the type $\eta_{12}\eta_{34}$, each with unit coefficient. These terms represent the possibility of two distinct pairs interacting just once. Each of the four possible Y_{ijk} also appears in (3.103) with unit coefficient [note that each C_{ij} contains some Y's according to (3.97)]. These terms represent all possible interactions among three particles, with the fourth particle remaining undisturbed in the Fermi sea. The higher-order terms in the C_{ij} involve at least three interactions that excite all four particles above the sea. A given sequence of interactions in which the last interaction is between, say, particles 1 and 2, occurs in every C_{ij} except C_{12}. The factor $\frac{1}{5}$ in (3.103) is necessary in order to correct for this overcounting.

If we now substitute (3.99) and (3.102) into (3.103), and put ζ equal to η, we obtain

$$\Psi=\prod_{\text{pairs}}(1-\eta_{ij}). \quad (3.104)$$

So we have the same connection with the Jastrow method as in the three-body case. However, Ψ contains less information than C_{12}. Knowing C_{12}, one can calculate Ψ. But knowing Ψ is not sufficient to calculate

[38] S. A. Moszkowski, Phys. Rev. **140**, B283 (1965).
[39] J. W. Clark and P. Westhaus, Phys. Rev. **141**, 833 (1966).

C_{12}, and it is specifically C_{12} that is needed in the four-body calculation.

We can now use our solution for C_{34} to calculate W_4. We must put C_{34} into (3.95) to obtain $D(r_{34})$ and then evaluate (3.94) to obtain W_4.

The calculation of $D(r_{34})$ from (3.95) requires a fivefold integration. Straightforward numerical quadrature was found to consume a prohibitive amount of computer time. So we followed Kuriyama[32] and approximated $\eta(r)$ and $\zeta(r)$ by functions of the form

$$\eta(r)=(1+c_1)\exp(-c_2r^2)-c_1\exp(-c_3r^2), \quad (3.105)$$

$$\zeta(r)=(1+d_1)\exp(-d_2r^2)-d_1\exp(-d_3r^2), \quad (3.106)$$

where the c_i and d_i are adjusted to give good fits. The integrand in (3.95) now becomes a sum of many Gaussian functions. Each term can be integrated analytically by using Cartesian coordinates for $\mathbf{r}_1$ and $\mathbf{r}_2$, with particles 3 and 4 kept fixed. Even with this simplification, the large number of terms to be handled makes computation rather slow. Calculation of $D(r_{34})$ for one value of r_{34} took 2.3 min on the CDC 3600 computer.

TABLE II. Values of parameters c_i and d_i used in (3.105) and (3.106). The constants c_2, c_3, d_2, and d_3 are given in units of F^{-2}, and c_1 and d_1 are dimensionless.

	c_1	c_2	c_3	d_1	d_2	d_3
Case 1	0.290	2.795	0.703	0.333	3.301	1.122
Case 2	1.278	2.165	1.332	0.333	3.301	1.122
Case 3	1.278	2.165	1.332	Same as c_i		
Case 4	0.565	2.536	0.629	0.338	3.237	1.110

Calculations were done for the four sets of c_i, d_i shown in Table II. The c_i in cases 1 and 2 both give a reasonably good fit to $\eta(r)$. The rms difference between $\eta(r)$ and (3.105) is about 0.02 in both cases, for $r<2F$. The corresponding rms differences for $\zeta(r)$ are about 0.01 in both cases. As expected, cases 1 and 2 give similar results, and the function $D(r_{34})$ for case 2 is shown in Fig. 48. In case 3, we put $\zeta(r)$ equal to $\eta(r)$. This approximation greatly simplifies the calculations, and it is therefore of interest to see how accurate it is. The result for $D(r_{34})$ is shown in Fig. 48. We see that putting $\zeta=\eta$ produces only a small error in $D(r_{34})$. In case 4, the c_i and d_i are fitted to the reference-spectrum[6,8] approximations to $\eta(r)$ and $\zeta(r)$, respectively. The resulting function $D(r_{34})$ is seen from Fig. 48 to be much too large (note that case 4 is plotted to a different scale in Fig. 48). The inadequacy of reference-spectrum wave functions for three-body calculations has been pointed out before.[16] This result is not surprising because the value of $\int\eta^2 d\tau$ is too large by a factor of 2 in the reference-spectrum approximation.

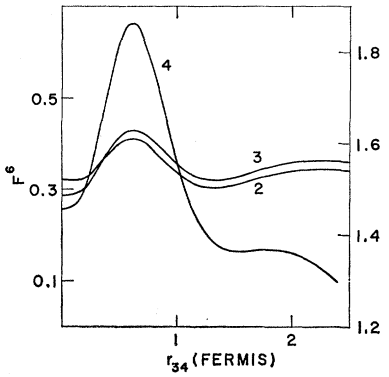

FIG. 48. Function $D(r_{34})$ that is needed in the calculation of W_4. Curve 2 is calculated using accurate approximations for $\eta(r)$ and $\zeta(r)$. Curve 3 is obtained by putting $\zeta(r)$ equal to $\eta(r)$. In curve 4, the reference-spectrum approximations for $\eta(r)$ and $\zeta(r)$ have been used. The left-hand vertical scale is used for curves 2 and 3, and the right-hand vertical scale is used for curve 4.

Having calculated $D(r_{34})$, we use (3.94) to compute W_4. Here, we must decide what values of k and γ^2 to use in calculating $g(r)$. We calculated for the two cases shown in Table III. The parameters of case 1 are appropriate for the three-body cluster calculation. For the four-body calculation, k and γ^2 should be larger by, very roughly, a factor of $\frac{4}{3}$. This leads to values similar to those of case 2. The resulting functions $g(r)$ are shown as curves 2 and 3 in Fig. 45 and differ only at short distances. The difference in W_4 between cases 1 and 2 is less than 10%. We conclude that W_4 is only moderately sensitive to the values of k and γ^2 used to calculate $g(r)$.

For $k=2.2$ F^{-1} and $\gamma^2=17.52$ F^{-2}, choices 1, 3, and 4 for the c_i and d_i gave $W_4=-0.12$, -0.11, and -0.45 MeV, respectively. The repulsive contribution to the integral (3.94) from $r<0.65$ F cancels 40% of the attractive contribution coming from larger r.

The value $W_4\approx-0.1$ MeV is quite reasonable. One would expect *a priori* that $W_4/W_2\approx\kappa^2$, where $W_2\approx-30$ MeV is the two-body contribution to the energy per particle. Since we have assumed the Reid $^1S_0$ potential to act in both the $^1S_0$ and $^3S_1$ states, we should use the corresponding value of κ, which is 0.044.[6] Then we find

$$W_4/W_2\approx 0.1/30=0.003, \quad (3.107)$$

$$\kappa^2=0.044^2\approx 0.002, \quad (3.108)$$

TABLE III. Values of k and γ^2 used in the calculation of $g(r)$ for four-body clusters.

	k (F^{-1})	γ^2 (F^{-2})
Case 1	1.8	12.72
Case 2	2.2	17.52

TABLE IV. Summary of numerical results, as discussed in the text.

Class	Rough analytic formula	Numerical result (soft core) (MeV)	Extrapolated result (hard-core) (MeV)
A1	$\frac{1}{2}\kappa^2\bar{U}$	−0.60	−1.15
A2	$-4\kappa W_3^{\rm hh}$	+0.18	+0.34
A3	$\propto\kappa^2$	+0.26	+0.53
A4	$\propto\kappa^2$	−0.22	−0.45
A5	$-2r\kappa\bar{U}^2/(9\bar{e})$	−0.15	−0.19
B1	$\propto\kappa^2$	−0.52	−1.06
B2	$\propto\kappa^2\bar{U}$	−0.20	−0.38
B3	$-3\kappa W_3$	+0.45	+0.64
B4	$\frac{1}{3}\kappa W_3$	−0.05	−0.07
W_4	$\propto\kappa^2$	−0.24	−0.49
	Total	−1.09	−2.28

and these two numbers are comparable, as expected. Another way of saying the same thing is to note that, taking $D(r_{34})$ to be constant, we have

$$W_4\approx(3/32)\rho^3 D\int g(r)\,d\tau, \tag{3.109}$$

$$W_2\approx\tfrac{3}{8}\rho\int g(r)\,d\tau. \tag{3.110}$$

Thus we expect to find that

$$W_4/W_2\approx\tfrac{1}{4}\rho^2 D=0.003, \tag{3.111}$$

and this is indeed borne out by actual calculation.

We have completely neglected the tensor force in our treatment of four-body clusters. In the three-body cluster calculation,[14] inclusion of the tensor force gives an additional contribution that is comparable to that coming from central forces alone. If the same thing holds true for four-body clusters, then W_4 will be only about −0.2 MeV, even when the tensor force is included. However, this is just a guess and should be checked by a detailed investigation.

Although Kuriyama's formulation[32] differs from ours (see the end of Sec. II C), his numerical results for W_4 are about the same as ours at normal density. He also finds W_4 to become rapidly more negative as the density is lowered. Lawson and Sampanthar[31] do not obtain a numerical result for W_4.

F. Summary of Numerical Results

The numerical results that have been obtained are summarized in Table IV. In the first column are listed the various classes of four-hole-line diagrams (W_4 refers to the four-body clusters). Classes A6–A9 and B5 and B6 have been omitted because their contributions are so small. The second column gives the analytic estimate of the contribution whenever such an estimate was made. In other cases (A3, A4, B1, B2, and W_4) the second column gives an idea of how the contribution scales with κ and $\bar{U}$.

The third column of Table IV gives our best numerical estimate of the contribution from each class, using the Reid[18] soft-core potential. The tensor force is properly included in all classes except B1, B2, and W_4. For each of these we have arbitrarily doubled the result obtained for central forces in order to include the effects of the tensor force.

In the fourth column of Table IV we estimate the contributions that would be obtained from the Reid[18] hard-core potential. These results are obtained by using the formulas in the second column to extrapolate the numerical results for the soft-core potential. In making these extrapolations, we have assumed that r, $\bar{e}$, and W_3 have the same values for the hard-core potential as for the soft-core potential. The values of κ for the hard- and soft-core cases are[6] 0.193 and 0.135, respectively, giving a ratio of 1.43. We have taken $\bar{U}=-66$ MeV (soft core) and $\bar{U}=-62$ MeV (hard core). This implies that the first-order binding energy is 2 MeV less for the hard core, as is reasonable.[6] In extrapolating W(A2) from soft core to hard core, we use the fact that $W_3^{\rm hh}$ is proportional to $\kappa\bar{U}$. These extrapolations are well justified in cases where an analytic estimate has been made. They are less certain in other cases (A3, A4, B1, B2, W_4), where we have simply made a reasonable guess about how the contribution scales with κ and $\bar{U}$.

The sum of all contributions is −1.09 MeV for the Reid soft-core potential. It is believed that all the calculated values are reliable except for those of classes B1, B2, and W_4, in which the main uncertainties come from the tensor force. If only the contributions to these three classes from central forces are included, the total four-hole-line energy is −0.61 MeV. If, for each of these three classes, the contribution from tensor forces is assumed to be twice that from central forces, then the total four-hole-line energy becomes −1.57 MeV. The truth probably lies somewhere between these extremes. So the total four-hole-line energy is probably between −0.6 and −1.6 MeV for the Reid soft-core potential. The result for the Reid hard-core potential is roughly twice as large as that for the soft core. A proper treatment of the tensor force is required in order to obtain a more precise result.

One more possible source of error is the value of W_3. The only complete calculation of W_3, including the tensor force, was carried out[14] by Dahlblom for the Reid hard-core potential. The four-hole-line energy contains the term $-(8\kappa/3)W_3=-0.36W_3$, coming from classes B3 and B4. If future calculations of W_3 for the soft-core potential give a value different from Dahlblom's result of −1.1 MeV, our numerical results will have to be changed accordingly.

Finally, we repeat our results for the contribution $W_3^{\rm hh}$ from the hole-hole diagram. An accurate calculation for the soft-core potential gives −0.34 MeV. The extrapolation to the hard-core potential gives −0.49 MeV, which we believe to be a reliable result.

IV. SUMMARY AND DISCUSSION

We have enumerated the four-hole-line diagrams and have given exact formal expressions for their contributions. In this procedure, a very important role is played by GTO, which collapses classes of diagrams into single diagrams and simplifies the energy denominators. In our formulas, all energy denominators are clearly defined, and exchange diagrams are fully taken into account. Although approximations must be made in any practical calculation, our exact formal expressions are still useful as a starting point for numerical work. Starting from the exact formulas, one can systematically introduce approximations until a practical formula is obtained.

We have given methods for making rough but quick estimates of most diagrams in terms of parameters such as κ, $\bar{U}$, etc. When checked by detailed calculation, these estimates are typically found to be in error by about 50%. Hence the rough estimates provide a reliable way of deciding that certain classes of diagrams give negligibly small contributions. We have used this method to show that the contributions from classes A6–A9 and B5 and B6 are too small to be of interest. A second virtue of the rough estimates is that they allow an extrapolation of numerical results for one two-body potential and particle density to other two-body potentials and particle densities. Our numerical results for the Reid soft-core potential have been extrapolated in this way to the Reid hard-core potential.

Our numerical work indicates that for the Reid soft-core potential, the total contribution from four-hole-line diagrams lies between -0.6 and -1.6 MeV per particle at normal density. We have not taken proper account of the tensor force in several classes of diagrams, and this is the main source of uncertainty in our numerical result. For the same density and two-body force, we have calculated the contribution from the hole-hole diagram (which has only *three* independent hole lines) to be -0.34 MeV per particle.

The main conclusion to be drawn from our numerical results is that the convergence of the hole-line expansion continues to be governed by the value of κ. For the Reid soft-core potential, we have $\kappa^2 W_2 = -0.6$ MeV, which is about half of our best estimate for the sum of all four-hole-line contributions. The possibility of obtaining a large result by summing many contributions, each one being of the order of $\kappa^2 W_2$, has not materialized. One reason for this is cancellation between attractive and repulsive contributions. The repulsive contributions listed in Table IV cancel about 45% of the attractive ones. A second reason is the presence, in almost all of the diagrams, of phase-space factors or of small statistical weights due either to exchange or to a diagram's having fewer than four closed loops. Because of these phase-space and statistical factors, 6 of the 16 classes of four-hole-line diagrams have negligible contributions, and only 3 classes give contributions of magnitude comparable to $\kappa^2 W_2$.

These phase-space and statistical factors will undoubtedly be extremely important in reducing the five-hole-line contribution to the energy. The number of distinct classes of five-hole-line diagrams is probably one or two hundred. Neglecting statistical and phase-space factors, the contribution of a typical class would be $\kappa^3 W_2 \approx 0.1$ MeV. But the statistical and phase-space factors may well reduce almost all of these terms by a factor of 10 or more, and there will certainly be substantial cancellation between attractive and repulsive contributions. Thus the five-hole-line energy could easily be very small, but we are unable to give any quantitative estimate without actually writing down the diagrams explicitly. This would be an enormous task. The hole-line expansion becomes inefficient if one is forced to carry it out to high order by brute force, and one should probably search for a more efficient procedure if one wants to go beyond four independent hole lines. In the meantime, what can we say about the accuracy of nuclear-matter calculations? Assuming that the error in the hole-line expansion is no larger than the last term calculated, a calculation that accurately includes all terms with two, three, and four independent hole lines will be uncertain by roughly 1 MeV for the Reid soft-core potential. The uncertainty will be larger for two-body potentials that give larger values of κ. To reduce the uncertainty much below 1 MeV is nearly impossible with the present methods.

It is very gratifying that the four-hole-line contribution to the energy is attractive and increases the total binding energy. All recent nuclear-matter calculations[6,26,40] have given binding energies that are several MeV smaller than the empirical value. The four-hole-line contributions will improve the agreement between the theoretical and empirical binding energies.

Our numerical work has focused particular attention on the diagrams of class B1. A proper treatment of the tensor force in these diagrams would greatly reduce the uncertainty in the four-hole-line energy.

The present work is incomplete in several respects. We have worked only at normal density and have considered only the Reid two-body potentials. The tensor force has been omitted from three important diagrams. We have also assumed that $U(k) = 0$ for $k > k_F$. This gives a big gap in the energy spectrum at the Fermi surface. It has been suggested[41,42] that a better single-particle spectrum would be nearly continuous at $k = k_F$ and would approach pure kinetic energy only at

[40] D. W. Sprung, in Proceedings of the International Conference on Atomic Masses, University of Manitoba, Winnipeg, 1967 (unpublished).

[41] Reference 23, p. 805.

[42] M. Baranger, in *Proceedings of the International School of Physics "Enrico Fermi," Course XL*, edited by M. Jean (Academic Press Inc., New York, 1969), p. 582.

large k, say $k>2k_F$. If this idea turns out to be right, some of the approximations that we have used may become unreliable. For example, the approximation of neglecting the dependence of κ_{lm} on the momenta of states l and m will certainly become much worse. The numerical work will then become more difficult. Making the single-particle potential attractive for low-lying unoccupied states will also increase[26] the value of κ and therefore worsen the convergence oi the energy expansion.

ACKNOWLEDGMENTS

I am grateful to H. A. Bethe for his encouragement in this work. Discussions with B. Brandow and F. Coester are greatly appreciated. I want to thank R. V. Reid for sending me his nucleon-nucleon potentials before publication, and J. MacKenzie for allowing me to use his computer subroutines for Gauss integration. A. Kuriyama kindly explained to me in a letter some of the details of his four-body calculation.

PHYSICAL REVIEW VOLUME 187, NUMBER 4 20 NOVEMBER 1969

Be^8 States at 16.6 and 16.9 MeV and Final-State Coulomb Interactions*

F. D. INGRAM† AND E. NORBECK

Department of Physics and Astronomy, The University of Iowa, Iowa City, Iowa 52240

(Received 13 June 1969)

The shape, width, and location of the 16-MeV resonances in the α-particle energy spectrum from the $Li^6(Li^6, \alpha)Be^8$ reaction were found to be a function of the angle taken by the breakup fragments in the subsequent decay of the Be^8. This was caused by the long-range electrostatic interaction between the α particle and the breakup particles.

I. INTRODUCTION

THE effects of final-state Coulomb interactions were studied with the reaction $Li^6(Li^6, \alpha_0)Be^8$, where the Be^8 was left in the 16.6- and 16.9-MeV states and where the Li^6 beam energy was 6 MeV. Preliminary results from this work have been described under the title, "Distortion of Nuclear Spectra by Final-State Coulomb Interactions".[1] It was shown that effects of this kind can be important in many nuclear reactions and are particularly important when precision measurements are made on unbound nuclear levels. If corrections for these effects were applied to the values in the literature, some of the energy levels would need to be lowered slightly and made more narrow.

The lifetimes of the two Be^8 states are such that, on the average, the α_0 particles are about 100 F (10^{-11} cm) away from the Be^8 before it disintegrates. At this distance the electrostatic potential energy of the Be^8-α_0 system is 115 keV. When the Be^8 breaks up in a direction perpendicular to the direction of α_0, the α_0 does not get its full share of this energy. The energy lost is about 30 keV.

An effect that is five times larger occurs when the Be^8 breaks up in a direction roughly parallel to the direction taken by α_0. In this case α_0 gains energy because the breakup particle follows along behind α_0, allowing the electrostatic repulsion to occur over a very long time.

At all angles, calculations using classical mechanics were found to agree moderately well with the experimental energy shifts. The calculation for the change in the widths as a function of angle were uncertain by as much as a factor of 2 at some angles because of the difficulties of using classical mechanics for what is really a quantum-mechanical problem. The experiment was not designed to make precise measurements of the widths.

II. EXPERIMENTAL TECHNIQUES

The 6-MeV Li^6 beam from the University of Iowa Van de Graaff was used to bombard thin Li^6F targets which had been evaporated onto 190-nm nickel foil. The α_0 particles were detected with a 50-mm², 150-μ surface-barrier silicon detector placed at an angle of 15° with respect to the beam direction. An aperture, placed in front of the detector, limited the acceptance angle from the center of the target chamber to 3°. All of the detectors were covered by 5.2-mg/cm² nickel foil to stop scattered beam. The detectors were calibrated with a 10.6-h Th B preparation that emitted 6.05- and

* Supported in part by the National Science Foundation.

† Present address: Department of Physiology and Biophysics, The University of Iowa, Iowa City, Iowa 52240.

[1] E. Norbeck and F. D. Ingram, Phys. Rev. Letters 20, 1178 (1968).